Eur. Phys. J. C 51, 83–101 (2007)
DOI 10.1140/epjc/s10052-007-0293-8

THE EUROPEAN PHYSICAL JOURNAL C

Regular Article – Theoretical Physics

Nonperturbative and perturbative aspects of photo- and electroproduction of vector mesons

H.G. Dosch[1,a], E. Ferreira[2,b]

[1] Institut für Theoretische Physik, Universität Heidelberg, Philosophenweg 16, 6900 Heidelberg, Germany
[2] Instituto de Física, Universidade Federal do Rio de Janeiro, Rio de Janeiro 21945-970, RJ, Brazil

Received: 15 September 2006 / Revised version: 15 March 2007 /
Published online: 28 April 2007 –

Abstract. We discuss various aspects of vector meson production, first analysing the interplay between perturbative and nonperturbative aspects of the QCD calculation. Using a general method adapted to incorporate both perturbative and nonperturbative aspects, we show that nonperturbative effects are important for all experimentally available values of the photon virtuality Q^2. We compare the huge amount of experimental information now available with our theoretical results obtained using a specific nonperturbative model without free parameters, showing that quite simple features are able to explain the data.

1 Introduction

Electroproduction of vector mesons provides an interesting laboratory for studying the interplay between perturbative and nonperturbative QCD. Most emphasis has been put on the perturbative side of the calculations [1–10]. In these calculations the production process is considered to be mediated by two-gluon exchange, and the coupling of the gluons to the hadron, generally a proton, is taken from a phenomenologically determined gluon distribution as obtained from deep inelastic scattering (DIS). The coupling of the exchanged photons to the produced quarks is treated perturbatively. This is justified if there is a truly hard scale and the produced quarks stay close together.

The emphasis put on perturbation theory is understandable given its justification in terms of the basic elements of QCD. Nevertheless, we think it is useful and even necessary to scrutinise also the other side of the medal, namely the nonperturbative aspects, and investigate its consequences. To examine the roles and magnitudes of different effects we have chosen an approach that starts from general expressions and investigate the limit of where perturbation theory holds. We derive and discuss particularly the deviations from perturbative QCD induced by nonperturbative effects.

There are several important reasons for this approach.

- Even if the produced vector mesons are heavy, the effect of binding by a confining potential is not negligible at presently accessible values of the photon virtuality Q^2. The binding effect influences very strongly the Q^2 dependence of the production amplitude.
- Even for high values of Q^2 the production of transversely polarised vector mesons receives important contributions from regions where the two produced quarks are widely separated.
- In spite of a clear transition from the perturbative to the nonperturbative regime, there are nevertheless striking systematic features in the production of light and heavy vector mesons, whose understanding requires the incorporation of nonperturbative methods.
- The gluon distribution of the proton as obtained from DIS allows one only to calculate production amplitudes with zero momentum transfer. This requires quite essential extrapolations in the analysis of the experimental data. Since the approach discussed here is based on a space-time picture it automatically takes skewing effects into account, and therefore the dependence of the production amplitude on (moderate) values of t, the momentum transfer from the virtual photon to the proton, can be calculated.
- In QCD the production of vector mesons is closely related to purely hadronic scattering processes without requiring the use of vector dominance models. In order to obtain a unified picture, it is clearly necessary to handle nonperturbative effects.
- Closely related to the previous item is the relation between QCD and Regge theory. In order to investigate possible bridges between the two approaches, again nonperturbative methods must be used.

The calculation of photo- and electroproduction presented in this paper uses a general method for high energy scattering based on the functional integral approach to QCD and on the WKB method that is capable of incorporating both the perturbative and nonperturba-

[a] e-mail: H.G.Dosch@thphys.uni-heidelberg.de
[b] e-mail: erasmo@if.ufrj.br

tive aspects [11, 12]. The nonperturbative input is given by a special model of nonperturbative QCD, called the stochastic vacuum model [13, 14], which has been successfully applied in many fields, from hadron spectroscopy to high energy scattering. The very satisfactory results of the model in purely nonperturbative regions gives strong weight to our determination of nonperturbative correction terms near the perturbative regime. The energy dependence is based on the two-pomeron model of Donnachie and Landshoff [15].

In previous papers we investigated photoproduction [16] and electroproduction [17] of J/ψ vector mesons. We have also used the same framework to investigate some general features of photo- and electroproduction of all S-wave vector mesons [18] that arise from the structure of the overlaps of photon and vector meson wave functions.

In recent years many more data have been obtained in HERA experiments, with higher accuracy and statistics, and their comparison with theoretical calculations provides opportunities to understand and describe important general features of the dynamics governing these processes. In particular, we may learn to what extent the experimentally observed features are contained in the global nonperturbative aspects of the systems in the final and initial states, such as their wave functions and the long range correlation properties of the intervening forces. In this paper we describe very successfully most of these recent data, using the same framework as the one that has been tested in several other cases, without the introduction of any free parameter.

Our paper is organised as follows.

In Sect. 2 we describe the methods used in the theoretical calculations of photo- and electroproduction of vector mesons. Since this has already been done on several occasions, we only give a short and schematic description and then focus attention on the comparison with the usual perturbative treatment.

In Sect. 3 we present the results of our calculations of photo- and electroproduction of all $1S$-wave vector mesons and compare them with the experimental data. We show that the predictions for all observables, the absolute values as well as the dependence on the photon virtuality Q^2, the momentum transfer t and the energy W, are very satisfactory.

After a short review of some related work, in the summary we comment on our results and present them in context.

The appendix gives formulas and details of the theoretical calculations and presents some of their general properties.

2 General formulæ and the strictly perturbative limit

We start from a general approach to scattering based on functional integrals and the WKB approximation [11, 12] that has been adapted to hadron–hadron scattering [19, 20] and to photo- and electroproduction of vector mesons

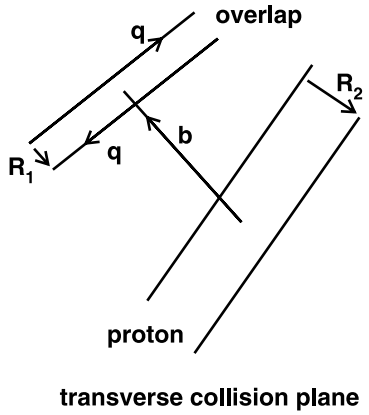

Fig. 1. Loop–loop scattering

hadrons [16, 17, 21]. The basic features can be seen in Fig. 1, which represents the loop–loop scattering amplitude in real space-time. The space-time trajectory of the photon is represented by a quark–antiquark loop, that of the proton by a quark–diquark loop. The transition to observable electroproduction amplitudes of hadrons is achieved through a superposition of the loop–loop amplitudes with the light cone wave functions of the hadrons and the photon used as weights. This leads to an electroproduction amplitude of the form

$$T_{\gamma^* p\to Vp,\lambda}(W,t;Q^2) = (-2\mathrm{i}W^2)\int \mathrm{d}^2R_1\,\mathrm{d}z_1\psi_{V\lambda}(z_1,R_1)^* \times \psi_{\gamma^*\lambda}(z_1,R_1,Q^2)J(\mathbf{q},W,z_1,\mathbf{R}_1)\,, \tag{1}$$

with

$$J(\mathbf{q},W,z_1,\mathbf{R}_1) = \int \mathrm{d}^2R_2\,\mathrm{d}^2b\mathrm{e}^{-\mathrm{i}\mathbf{q}.\mathbf{b}}|\psi_p(R_2)|^2 \times S(b,W,z_1,\mathbf{R}_1,z_2=1/2,\mathbf{R}_2)\,. \tag{2}$$

Here $S(b,W,z_1,\mathbf{R}_1,1/2,\mathbf{R}_2)$ is the scattering amplitude of two dipoles with separation vectors $\mathbf{R}_1$, $\mathbf{R}_2$, colliding with impact parameter vector $\mathbf{b}$; $\mathbf{q}$ is the momentum transfer vector of the reaction, with

$$t = -\mathbf{q}^2 - m_p^2(Q^2+M_V^2)/W^4 + O(W^{-6}) \approx -\mathbf{q}^2\,. \tag{3}$$

In these expressions $Q^2 = -p_{\gamma^*}^2$ is the photon virtuality, W is the center of mass energy of the γ^*–proton system, and $t = (p_V - p_{\gamma^*})^2$ is the invariant momentum transfer from the virtual photon to the produced vector meson; z_1 is the longitudinal momentum fraction of the quark in the virtual photon and in the vector meson, and we define $\bar{z}_1 = 1 - z_1$; the $\psi(z,\mathbf{R})$ represent the light cone wave functions.

The differential cross section is given by

$$\frac{\mathrm{d}\sigma}{\mathrm{d}|t|} = \frac{1}{16\pi W^4}|T|^2\,. \tag{4}$$

For the special case of forward production ($\mathbf{q}=0$) this approach reduces to the dipole model for electroproduction [22, 23].

Details of the evaluation of the loop–loop amplitude in the stochastic vacuum model can be found in previous publications [16, 21].

2.1 The perturbative limits and nonperturbative corrections

For the photon wave functions $\psi_{\gamma^*\lambda}(z_1, R_1, Q^2)$ we use the well known lowest order expressions, keeping the same notation as used before [16, 17].

If we concentrate on high values of the virtuality Q^2, the two valence quarks stay close together and we may use the dipole cross section of a small object of size R_1; that is,

$$J(\mathbf{q}=0, W, z_1, \mathbf{R}_1) = C(W, Q^2) R_1^2 \,. \tag{5}$$

If we furthermore ignore the transverse extension of the vector mesons, replacing

$$\psi_{V\lambda}(z_1, R_1) \to \psi_{V\lambda}(z_1, 0)\,, \tag{6}$$

we can perform the R_1 integration in (1) explicitly.

Later we introduce specific ansätze for the vector meson wave functions $\psi_{V\lambda}(z_1, R_1)$ and use the results of a specific model, the stochastic vacuum model, for the evaluation of the loop–loop scattering amplitude $J(\mathbf{q}, W, z_1, \mathbf{R}_1)$, but for the moment we stick to the general formulae and first study the corrections to the strictly perturbative limit.

We first consider the simpler case of *longitudinally polarised* photons, where we obtain with the replacement (6) (for later discussion we keep the dependence on the quark mass m_f in our expressions)

$$T^{\rm pert}_{\gamma^* p\to Vp,\lambda=0} = -(2{\rm i}W^2)16C(W,Q^2)\hat{e}_f\frac{\sqrt{3\alpha}}{2\pi}Q \times \int_0^1 {\rm d}z_1 \frac{8\pi z_1^2\bar{z}_1^2}{(z_1\bar{z}_1Q^2+m_f^2)^2}\psi_{V0}(z_1,0)\,. \tag{7}$$

The wave function at the origin $\psi_{V0}(z_1, 0)$ is related to the coupling of the vector meson to the electromagnetic current f_V by

$$f_V = \hat{e}_V\sqrt{3}\frac{1}{\sqrt{4\pi}}\int_0^1 {\rm d}z_1 16 z_1\bar{z}_1\psi_{V0}(z_1,0)\,. \tag{8}$$

Here $\hat{e}_f$ is the quark charge, and $\hat{e}_V$ is the effective charge in the meson, which is $\hat{e}_V = 1\sqrt{2}$ for the ρ and $\hat{e}_V = 1/3\sqrt{2}$ for the ω meson, while for the ϕ, ψ and Υ mesons we have $\hat{e}_V = \hat{e}_f$.

We introduce

$$\eta_{\rm L}(Q^2) = (Q^2/4+m_f^2)^2\frac{\int_0^1 {\rm d}z_1 \frac{4z_1^2\bar{z}_1^2\psi_{V0}(z_1,0)}{(z_1\bar{z}_1Q^2+m_f^2)^2}}{\int_0^1 {\rm d}z_1 z_1\bar{z}_1\psi_{V0}(z_1,0)} \tag{9}$$

and then write the perturbative expression as

$$T^{\rm pert}_{\gamma^* p\to Vp,\lambda=0} = (-4\pi{\rm i}W^2) f_V\sqrt{\frac{\alpha}{\pi}}\frac{\hat{e}_f}{\hat{e}_V}\eta_{\rm L}(Q^2) \times \frac{Q}{(Q^2/4+m_f^2)^2}C(W,Q^2)\,. \tag{10}$$

Noting that the longitudinal wave function is suppressed at the end points $z_1 = 0$ and $z_1 = 1$, we see that in the limit $Q^2 \to \infty$ the mass m_f can be neglected against $z_1\bar{z}_1Q^2$ and the expression $\eta_{\rm L}$ becomes independent of Q^2

$$\eta_{\rm L} \to \frac{\int_0^1 {\rm d}z_1\psi_{V0}(z_1,0)}{4\int_0^1 {\rm d}z_1 z_1\bar{z}_1\psi_{V0}(z_1,0)}\,. \tag{11}$$

This is the correction factor due to the longitudinal extension of the meson as obtained in [3] (up to a factor 2 due to different definitions). However, for practical purpose we keep using the expression (9) with finite quark masses. If there were no binding effects, z_1 would be $1/2$, and therefore $\eta_{\rm L}$ would approach 1 for Q^2 going to infinity.

Comparing (10) with the perturbative expression for the longitudinal electroproduction of vector mesons [3], we obtain

$$C(W,Q^2) = \frac{\pi^2}{3}xG(x,Q^2)\alpha_{\rm s}(Q^2)\,, \tag{12}$$

where x is the Bjorken variable, $x = (Q^2+M_V^2)/W^2$. This yields the well known relation between the dipole cross section and the gluon density [24]. After introducing our specific model for the meson wave functions in Sect. 2.3 we will present numerical values for $\eta_{\rm L}(Q^2)$, which represents the longitudinal momentum correction to the pure perturbative calculation of the amplitude for longitudinal photons.

Nonperturbative effects also lead to a finite extension of the vector meson and to a deviation of the simple quadratic behaviour of the "dipole cross section" $J(\mathbf{q}=0, W, z_1, R_1)$ in (5). We present numerical values for the rather large corrections due to these effects in Sect. 2.3.

As it is well known, the treatment of the *transverse polarisation* is more delicate for at least two reasons.

- There is no strong suppression of the photon wave function at the end points $z_1 = 0,\ z_1 = 1$ and therefore the effective scale, namely $z_1\bar{z}_1Q^2$, might be quite low even for highly virtual photons. This makes among other things a systematic $1/Q^2$ analysis impossible, since the factor corresponding to (11) diverges due to the singularities at the end points $z_1 = 0,\ 1$.
- The meson wave function is supposed to be more complicated, and relativistic contributions are likely to be important even for rather heavy mesons.

For simplicity we assume that the wave function of the vector meson has the same tensor structure as the transverse photon. Then the overlap function (1) with the replacement (6) brings about the form

$$T^{\rm pert}_{\gamma^* p\to Vp,\lambda=1} = -2{\rm i}W^2C(W,Q^2)\hat{e}_f\frac{\sqrt{6\alpha}}{2\pi} \times \int_0^1 {\rm d}z_1 \frac{4m_f^2\psi_{V1}(z_1,0)+16\omega^2(z_1^2+\bar{z}_1^2)\psi^{(1)}_{V1}(z_1,0)}{(z_1\bar{z}_1Q^2+m_f^2)^2}\,, \tag{13}$$

where

$$\psi_{V1}^{(1)}(z_1,0) = \frac{-1}{2\omega^2}\left(\frac{\partial}{\partial(R_1^2)}\psi_{V1}\right)(z_1,0)\,. \tag{14}$$

The relation to the decay constant f_V is here given by

$$f_V = \hat{e}_V \frac{\sqrt{6}}{M_V}\frac{1}{\sqrt{4\pi}} \times \int_0^1 \mathrm{d}z_1 \frac{m_f^2\,\psi_{V1}(z_1,0) + 2\omega^2(z_1^2+\bar{z}_1^2)\psi_{V1}^{(1)}(z_1,0)}{z_1\bar{z}_1}\,. \tag{15}$$

This leads to a relativistic correction factor η_T which is of order $O(\omega^2/m_f^2)$, given by

$$\eta_\mathrm{T}(Q^2) = (Q^2/4+m_f^2)^2 \times \frac{\int_0^1 \mathrm{d}z_1 \frac{4m_f^2\psi_{V1}(z_1,0)+16\omega^2(z_1^2+\bar{z}_1^2)\psi_{V1}^{(1)}(z_1,0)}{(z_1\bar{z}_1Q^2+m_f^2)^2}}{\int_0^1 \mathrm{d}z_1 \frac{4m_f^2\psi_{V1}(z_1,0)+8\omega^2(z_1^2+\bar{z}_1^2)\psi_{V1}^{(1)}(z_1,0)}{4z_1\bar{z}_1}}\,. \tag{16}$$

The final result for the transverse polarisation is written analogous to (10); that is,

$$T^\mathrm{pert}_{\gamma^*p\to Vp,\lambda=1} = (-4\pi\mathrm{i}W^2) f_V \sqrt{\frac{\alpha}{\pi}}\frac{\hat{e}_f}{\hat{e}_V}\eta_\mathrm{T}(Q^2) \times \frac{Q}{(Q^2/4+m_f^2)^2} C(W,Q^2)\,. \tag{17}$$

Only in the absence of binding effects it would be $\omega = 0$, $z_1 = \frac{1}{2}$, and we would then have $\eta_\mathrm{T}(Q^2) \to 1$ for $Q^2 \to \infty$, as it is in the case of longitudinal polarisation. Numerical values for the correction coefficients $\eta_\mathrm{T}, \eta_\mathrm{L}$ evaluated in a specific model are given in Sect. 2.3. Strong deviations of η_L and η_T from unity indicate important deviations of the amplitudes from the pure perturbative calculation, due to the longitudinal momentum in the photon–meson overlap and to relativistic effects.

Important additional corrections arise from the finite extension of the vector mesons, and they are also discussed in Sect. 2.3.

2.2 The specific nonperturbative model

In order to obtain numerical information on the corrections discussed in the two previous subsections, we need to use models both for the wave functions and for the interaction of gluons and hadrons.

The photon enters through its usual perturbative wave function. In model calculations [25] it has been shown that the perturbative wave function can be used also for small values of $Q^2+m_f^2$ if an appropriate constituent mass is introduced. For light mesons, the masses have been determined by comparison with the phenomenological two point function for the vector current. The approach has been successfully applied in the theoretical calculation of structure functions, Compton amplitudes and photon–photon scattering.

The wave function has been adapted from photons to vector mesons including relativistic corrections motivated by the structure of the vector current [17, 21, 25, 26]. As in previous papers [16, 17], we use two forms of meson wave functions: the Bauer–Stech–Wirbel (BSW) [27, 28], and the Brodsky and Lepage (BL) [29, 30] forms, which are given details of in the appendix. We use this type of wave function for all vector mesons, with quark masses determined from a best fit to the vector current (the masses are $m_u = m_d = 0.2$, $m_s = 0.3$, $m_c = 1.25$, $m_b = 4.2\,\mathrm{GeV}$).

Our nonperturbative treatment of the high energy process is based on functional integration [11, 12] and on the stochastic vacuum model [13, 14]. The method has been described in several occasions [20, 31, 32], and we only quote here a few of its characteristic features. The model is based on the assumption that nonperturbative QCD can be approximated by a Gaussian process in the colour field strengths; the gluon field correlator is therefore the quantity determining the full dynamics. Its parameters are taken from lattice calculations [33]. The model yields confinement in non-Abelian gauge theories and leads to realistic quark–antiquark potentials for heavy quarks [32]. It can be used to determine the loop–loop scattering amplitudes mentioned in the introduction and visualised in Fig. 1.

For the energy dependence we have introduced in the model [16, 34–36] the two-pomeron scheme of Donnachie and Landshoff [15]. Small dipoles couple to the hard, and large dipoles to the soft pomeron. The transition radius was determined through the investigation of the proton structure function. Again we refer to the literature for more information and collect some details and the relevant parameters in the appendix.

2.3 Numerical results for the nonperturbative corrections

In order to exhibit the importance of the nonperturbative contributions we display their effects explicitly in this subsection. We hasten to add that for the final calculations as given in Sect. 3 we do not split our results into perturbative and nonperturbative parts but give directly the full theoretical results.

The correction factors η_L (9) and η_T (16) are displayed in Fig. 2 as functions of $Q^2+4m_f^2$ for several vector mesons. The factor η_L reflects the effect of the distribution of the longitudinal momentum; we notice that it remains of order 1, and its influence is rather weak. In contrast, the correction in the transverse amplitude due to the factor η_T, reflecting mainly relativistic corrections to the transverse wave function, is very important, especially for high values of $Q^2+m_f^2$. Its large values at high Q^2 for the production of ρ mesons indicate that the measurement of the ratio of the longitudinal to the transverse production cross sections tests mainly the wave function. According to our calculations, only the quantity η_T for light mesons is very sensitive to the specific choice of the wave function.

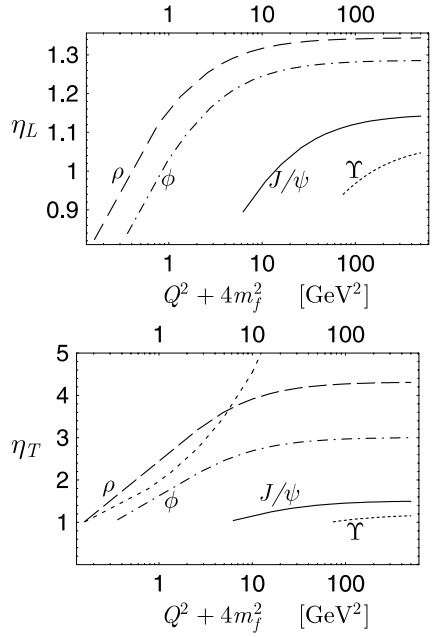

Fig. 2. Correction factors $\eta_{\rm L}$ (9) and $\eta_{\rm T}$, (16) due to the longitudinal momentum distribution in the longitudinal and transverse wave function of the mesons. The factors are similar for the BL and BSW wave functions, except for $\eta_{\rm T}$ for light mesons. The differences in these cases are illustrated by the comparison of the *long-dashed* and *short-dashed curves* corresponding to the BL (*long-dashed*) and the BSW (*short-dashed*) wave functions for the ρ-meson

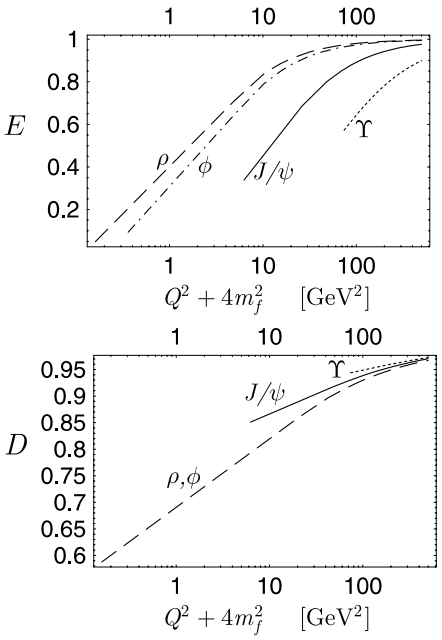

Fig. 3. Correction factors in the evaluation of the amplitudes for electroproduction. The factor E in the upper panel is due to the finite extension of the meson wave function, and the correction factor D in the lower panel is due to nonperturbative corrections to the simple R_1^2 dependence of the dipole cross section. The factors are very similar for longitudinal and transverse polarisations

There are large effects due to the finite extensions of the mesons. We denote by E the ratio of the full amplitudes (1) to the purely perturbative ones, (10) and (17). The ratio E is displayed in Fig. 3, left; the results for both polarisations are very similar. The effects are by no means negligible, even for the heavy mesons. The suppression due to the finite extension at low values of Q^2 leads, in the full range of the presently available data, to a much weaker decrease in Q^2 than inferred from purely perturbative expressions.

For large values of the quark–antiquark separation R_1, the dipole cross section differs from the pure R_1^2 behaviour as given by (5) and (12). We denote by D the ratio of production amplitudes of the more realistic dipole cross section obtained with the stochastic vacuum model divided by the result obtained with the purely quadratic expression (5). This factor D is displayed in Fig. 3, right; we see that it is important only for the light mesons at low values of Q^2. Also D is similar for the longitudinal and transverse polarisation.

The importance of nonperturbative contributions to vector meson photoproduction has been stressed before [37], using a different approach to nonperturbative corrections.

3 Theoretical results and comparison with experiment

A detailed description of the framework of our calculations can be found in our previous papers [16–18, 21]. The basis for the determination of the loop–loop scattering amplitude represented in Fig. 1 is the model of the stochastic vacuum. The calculations are determined by two parameters, the correlation length of the nonperturbative gluon fluctuations and the strength of the gluon condensate, which can be extracted from lattice calculations [33].

All parameters have been determined from other sources, and they are collected in Appendix A. Our calculations therefore contain no adjustable parameter, and all theoretical results are true predictions.

In the following we present a comparison of our theoretical results with the available data of elastic photo- and electroproduction of the S-wave vector mesons, namely $J/\psi, \Upsilon, \rho, \omega, \phi$.

3.1 Photo- and electroproduction of the J/ψ meson

In Fig. 4 we show the data for the integrated elastic cross section σ of J/ψ electroproduction at the fixed energy $W = 90$ GeV as a function of the photon virtuality Q^2. The data are from the Zeus [38, 39] and H1 [40] collaborations. The theoretical calculations (solid line) are made using the BL (Brodsky–Lepage) form of the vector meson wave function; the BSW wave function yields very similar results. The agreement between data and the theoretical calculations is remarkable. The dotted line in the figure, which nearly coincides with our theoretical calculation, is a fit to the data proposed in the experimental paper, with the

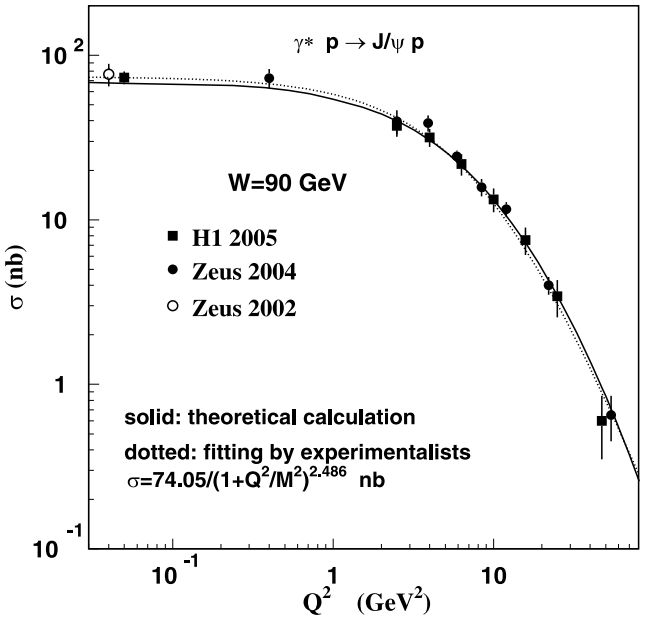

Fig. 4. Integrated elastic cross section of J/ψ photo- and electroproduction at the energy $W = 90\,\mathrm{GeV}$ as a function of Q^2. The data are from the Zeus [38, 39] and H1 [40] collaborations. The *solid line* represents our theoretical calculation using the BL wave function. The *dotted curve* is a pure fit to the experimental points of the form given by (18)

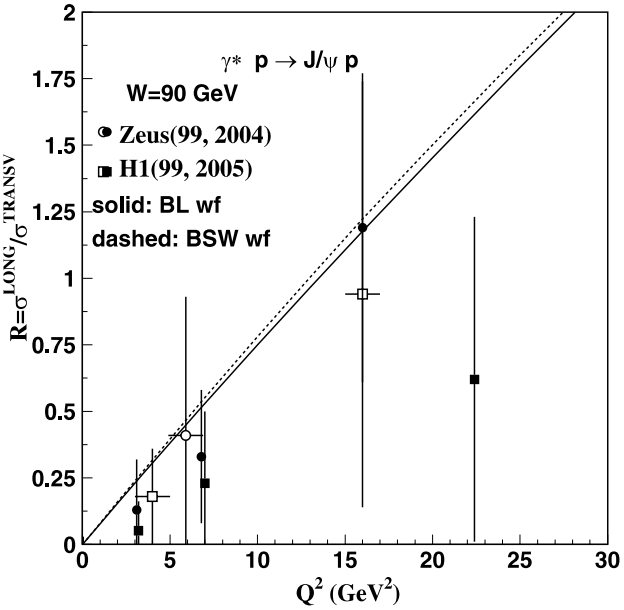

Fig. 5. The ratio R of longitudinal and transverse cross sections for J/ψ electroproduction as a function of Q^2 for the fixed energy of $W = 90\,\mathrm{GeV}$. Data are from the Zeus [39, 41] and H1 [40, 42] collaborations at HERA. The *solid line* and *dashed lines* show our theoretical calculations respectively with the BL (*solid*) and the BSW (*dashed*) wave functions. A good numerical representation for the BL result is $R(Q^2) \approx 0.76\,(Q^2/M^2)/(1+Q^2/M^2)^{0.09}$

usual form

$$\sigma = \frac{A}{(1+Q^2/M_V^2)^n}\,. \tag{18}$$

Figure 5 shows the ratio R of the longitudinal to the transverse cross sections,

$$R = \frac{\sigma^{\mathrm{L}}}{\sigma^{\mathrm{T}}}\,, \tag{19}$$

again for J/ψ elastic electroproduction at $W = 90\,\mathrm{GeV}$. As the ratio cancels influences of the specific dynamical model, this quantity directly tests details of the overlaps of wave functions, helping the study of their longitudinal and transverse structures The data are from the Zeus [39, 41] and H1 [40, 42] collaborations at HERA. As seen in the figure, the presently available data are not very accurate. The theoretical calculations with the two kinds of wave function – BL and BSW – give nearly the same results for $\sigma = \sigma^{\mathrm{L}} + \sigma^{\mathrm{T}}$ and for $R = \sigma^{\mathrm{L}}/\sigma^{\mathrm{T}}$.

Figure 6 shows the comparison of our calculations for the energy dependence of cross sections with the recent Zeus and H1 data [38–40] and older photoproduction data from fixed target experiments [43, 44] at lower energies. For illustration of our results for electroproduction we show data and theoretical results in the Q^2 range 6.8–7 GeV^2 for which there are both Zeus and H1 data.

Often the W dependence of the experimental cross sections is fitted through single powers in the form

$$\sigma = \mathrm{Const.} \times W^{\delta(Q^2)}\,, \tag{20}$$

which may be useful in limited W ranges. Values of the parameter δ obtained at several values of Q^2 in J/ψ electroproduction are compared to our theoretical predictions in Fig. 7, based on the two-pomeron scheme.

In contrast to purely perturbative approaches, our theoretical treatment allows one to calculate the dependence of the cross section on the momentum transfer t. The data on the t distribution in J/ψ photo [38, 40] and electroproduction [39, 40] at $W = 90\,\mathrm{GeV}$ are shown in Fig. 8 together with our theoretical results (solid lines). Also shown are electroproduction data and calculations at $Q^2 = 6.8$–$7\,\mathrm{GeV}^2$ for which measurements from both Zeus and H1 are available.

Our calculation predicts a curvature in the log plot for the t distribution that we may describe with the form

$$\frac{\mathrm{d}\sigma}{\mathrm{d}|t|} = \left[\frac{\mathrm{d}\sigma}{\mathrm{d}|t|}\right]_{t=0} \times F(|t|) = \left[\frac{\mathrm{d}\sigma}{\mathrm{d}|t|}\right]_{t=0} \times \frac{\mathrm{e}^{-b|t|}}{(1+a|t|)^2}\,. \tag{21}$$

For $\gamma^\star p \to p\psi$ at $W = 90\,\mathrm{GeV}$ our calculations at $Q^2 = 0$ give $a = 4.06\,\mathrm{GeV}^{-2}$ and $b = 1.75\,\mathrm{GeV}^{-2}$. The present data give no clear cut evidence for this curvature. The distribution becomes flatter as Q^2 increases, but in the investigated range it practically does not change with the energy (no shrinking).

In order to determine the integrated cross section the experimental data have to be extrapolated to the point of minimum momentum transfer. This brings a theoretical bias to the experimental points. It is therefore meaning-

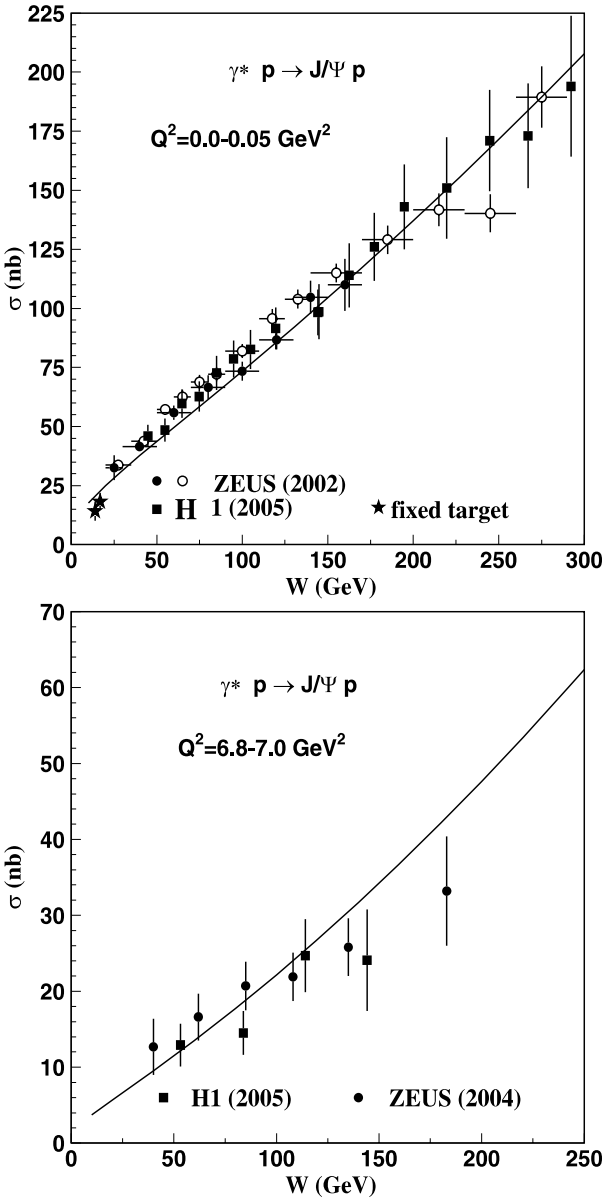

Fig. 6. Energy dependence of the integrated elastic cross section for J/ψ production from the HERA collaborations [38–40], compared with our theoretical calculations. The fixed target photoproduction data are from the E-401 and E-516 experiments [43, 44]. Electroproduction is represented by the Q^2 range 6.8–7.0 GeV^2, for which there are both Zeus and H1 data points

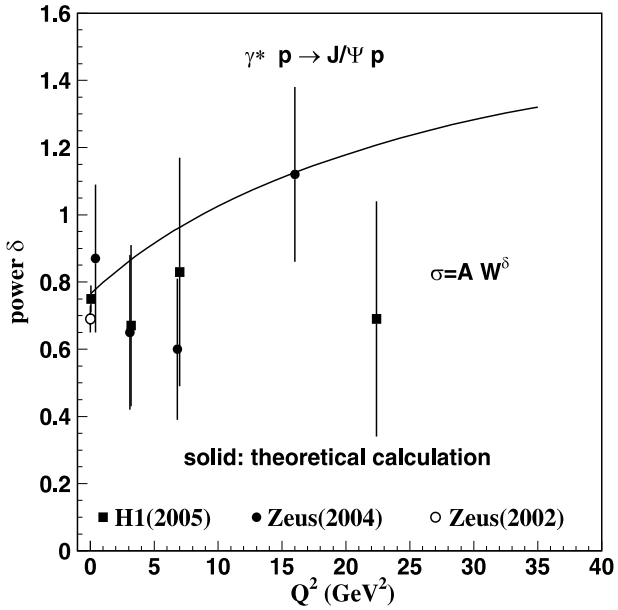

Fig. 7. Q^2 dependence of the δ parameter describing the energy dependence of the J/ψ integrated elastic cross section, from the Zeus and H1 collaborations [38–40], compared to our theoretical predictions

ful to compare our theoretical results with the observed data at small but finite momentum transfer. This is done in Fig. 9; the agreement is excellent.

3.2 Photo- and electroproduction of the Υ meson

For the Υ there are only two data points for photoproduction, at $\langle W \rangle = 120$ GeV [45] and $\langle W \rangle = 143$ GeV [46], shown together with our theoretical energy dependence in Fig. 10. In the second plot we show our calculation of the Q^2 dependence at the fixed energy $W = 130$ GeV, together with the data for $Q^2 = 0$ at the energies of 120 and 143 GeV. Both plots show a fairly good agreement with the data. It should be noted that, in spite of the high mass scale, the finite extension of the meson has a considerable effect, as it can be seen in Fig. 3, left.

3.3 Photo- and electroproduction of the ρ meson

The classical fixed target experiments [47–53] provide an important reference for the magnitudes of cross sections in ρ photo- and electroproduction at centre of mass energies of about 20 GeV. The data are shown in Fig. 11, together with the results of our calculation. The agreement is satisfactory, given the quite important discrepancies within the data in the interval $Q^2 = 4$–7 GeV^2.

Figure 12 shows the data for the integrated elastic cross section σ of ρ electroproduction at the fixed energy $W = 90$ GeV as a function of the photon virtuality Q^2. The data are from the Zeus [41, 54] and H1 [55, 56] collaborations. The solid line represents the theoretical calculations using the BL form of the vector meson wave function. Our theoretical calculations give a good overall description of the data but do not reproduce the details of the Q^2 dependence of ρ electroproduction as well as they did in J/ψ production. The present data indicate that in the ρ meson case a fitting of a simple form like (18) is not satisfactory for the whole Q^2 range. Two of such forms may be applied, with a transition in the values of both parameters (normalisation and power) occurring somewhere in the Q^2 range from 5 to 7. More experimental measurements are needed to clarify the structure of the data in this region, which

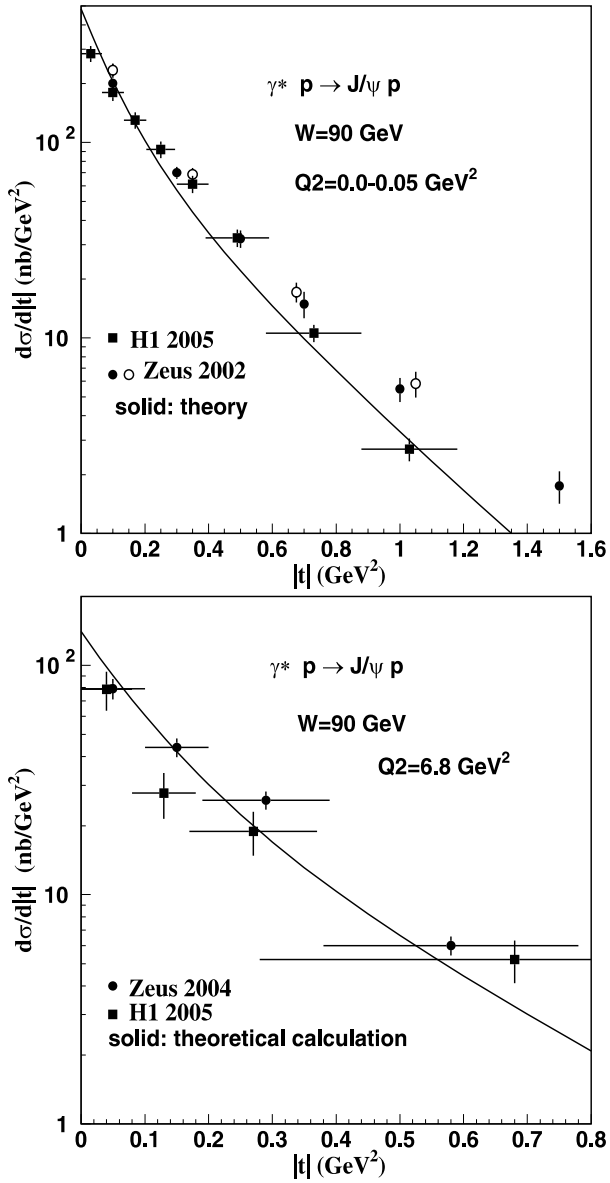

Fig. 8. The t dependence of the differential cross sections of J/ψ elastic photo- [38, 40] and electroproduction [39, 40]. The Zeus(2002) photoproduction results give separate information from events with ψ decaying into $\mu^+\mu^-$ (*full circles*) and e^+e^- (*empty circles*). The *solid lines* represent our theoretical results

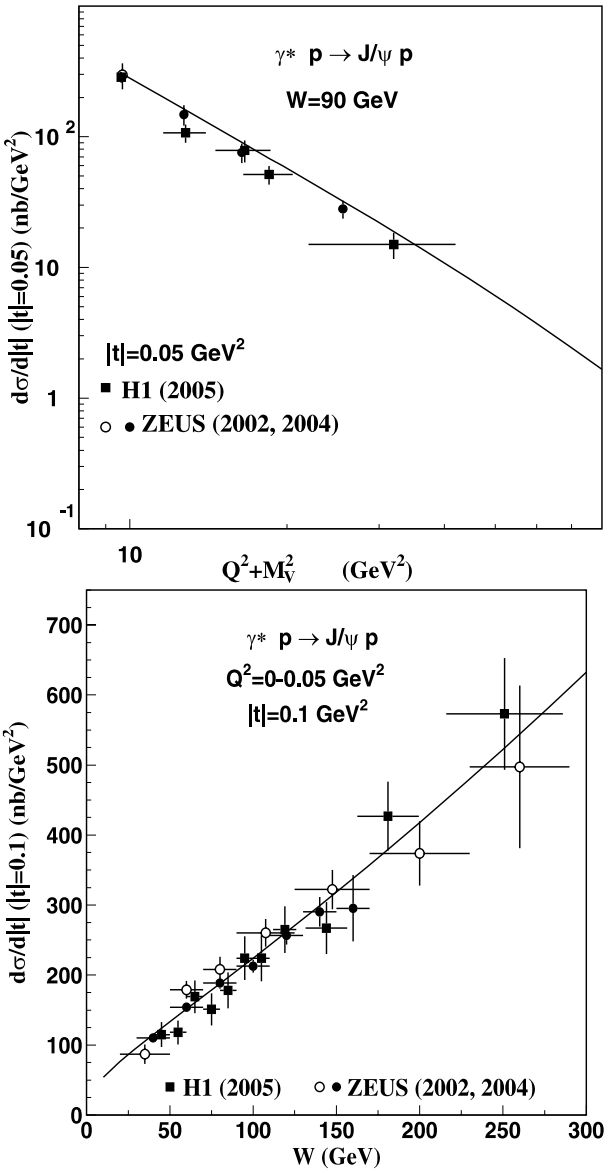

Fig. 9. Q^2 and W dependences of the (nearly) forward differential cross sections of J/ψ elastic photo- [38, 40] and electroproduction [39, 40]. The *solid lines* represent our theoretical results

may contain important information about the dynamics of the process.

Figure 13 shows the ratio $R = \sigma^{\mathrm{L}}/\sigma^{\mathrm{T}}$ of the cross sections for longitudinal and transverse polarisations for ρ elastic electroproduction at $W = 20$ and 90 GeV. The data at 90 GeV are from NMC [52, 53], Zeus [41, 54] and H1 [55–57]. The $W = 20$ GeV data are from the E-665 experiment [51]. To indicate the differences, the theoretical results for both BL (solid line) and BSW (dashed line) wave functions are displayed. For large Q^2, R becomes very sensitive to the values of the small transverse cross section. The measurement of this quantity R therefore provides important tests on the structure of the meson wave function.

Figure 14 shows the energy dependence of ρ electroproduction for several values of Q^2 together with our theoretical results. On the right-hand-side plot we show the effective power δ for the energy dependence (see (20)) for the W-region of approximately 30 to 130 GeV. The experimental points are from Zeus [41, 54, 58] and H1 [55, 56]. Our theoretical description, solid line, is very satisfactory within the experimental errors.

There are no published measurements of the differential cross section $\mathrm{d}\sigma/\mathrm{d}|t|$ in ρ production for nonzero values of Q^2. The Zeus photoproduction data at $W = 75$ and 94 GeV [58, 59] are shown in Fig. 15. In the low t range there are new preliminary data from H1 [60] at several energies. The numbers for the differential cross sections at 70 GeV for low t extracted from their plots are included in the figure,

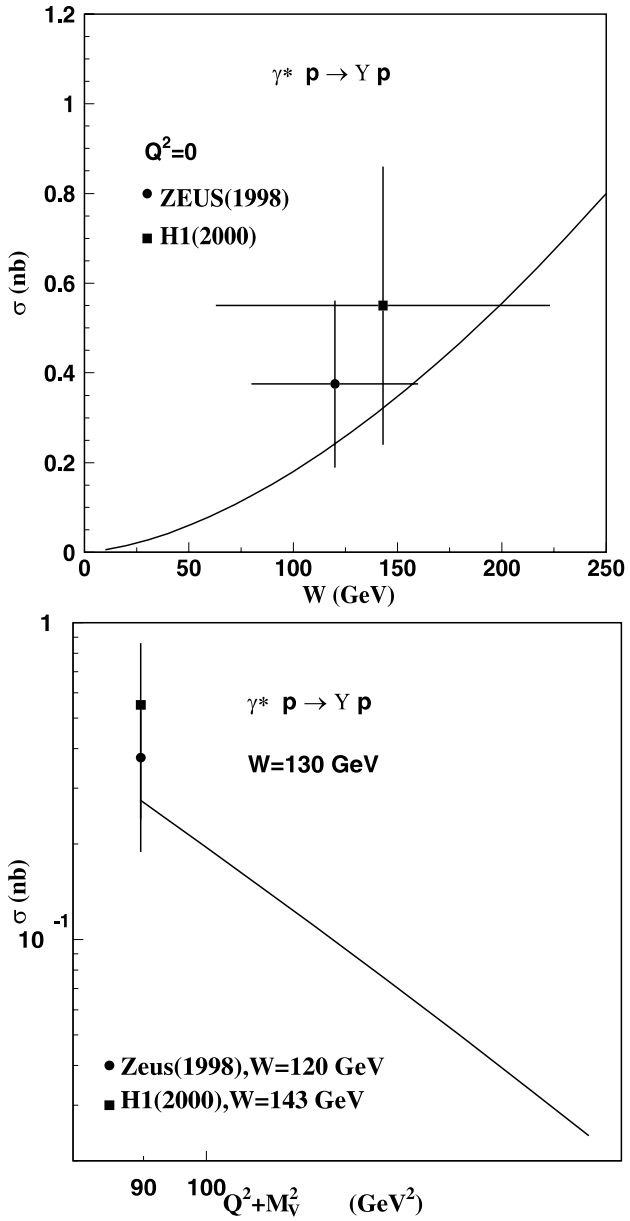

Fig. 10. Integrated elastic cross section of Υ photoproduction as a function of the energy and electroproduction at the energy $W = 130$ GeV as a function of Q^2. The data at the energies $\langle W \rangle = 120$ and 143 GeV are respectively from the Zeus [45] and H1 [46] collaborations. The *solid lines* represent our theoretical calculations using the BL wave function

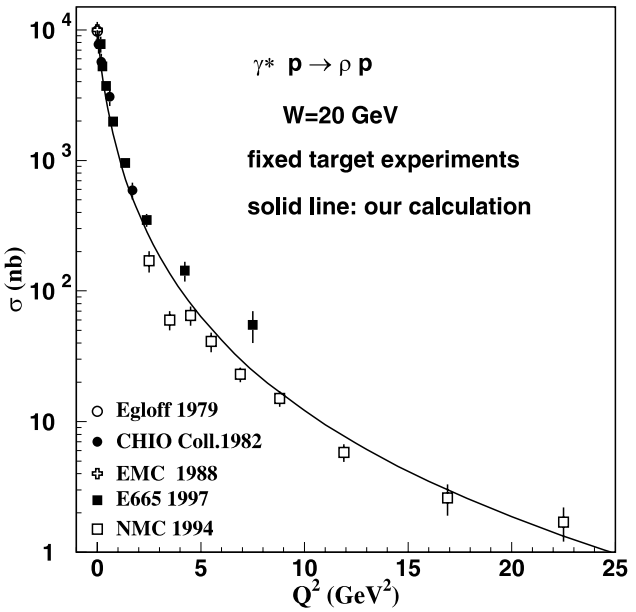

Fig. 11. Integrated elastic cross section for ρ electroproduction at the energy $W = 20$ GeV as a function of the photon virtuality Q^2. The data are from fixed target experiments [47–53], spanning almost two decades. The *solid line* represents the results of our calculations

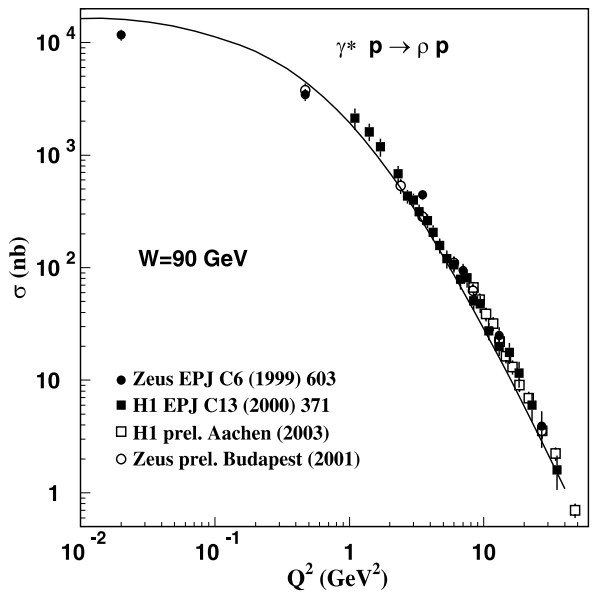

Fig. 12. Integrated elastic cross section of ρ electroproduction at the energy $W = 90$ GeV as a function of Q^2. The data are from the Zeus [41, 54] and H1 [55, 56] collaborations. The *solid line* shows our theoretical results using the BL wave function

and they seem to confirm the previous Zeus measurements at $W = 75$ GeV [58]. Our theoretical calculations are shown in the figures, and the description is satisfactory.

3.4 Photo- and electroproduction of the ω meson

As particles of about the same size and mass, ω and ρ have similar behaviours in the soft processes that we study here.

The Q^2 dependence of ω photo- and electroproduction [61, 62] is shown in Fig. 16. The agreement between our results and the data is not perfect, but satisfactory, in view of there being no free parameter involved in the calculations.

The existing data [63, 64] on the t dependence of the differential cross section in ω production are shown in Fig. 17. In the figure are put together the data points of the energies $W = 15$ GeV (with $Q^2 = 0$) and $W = 80$ GeV (with

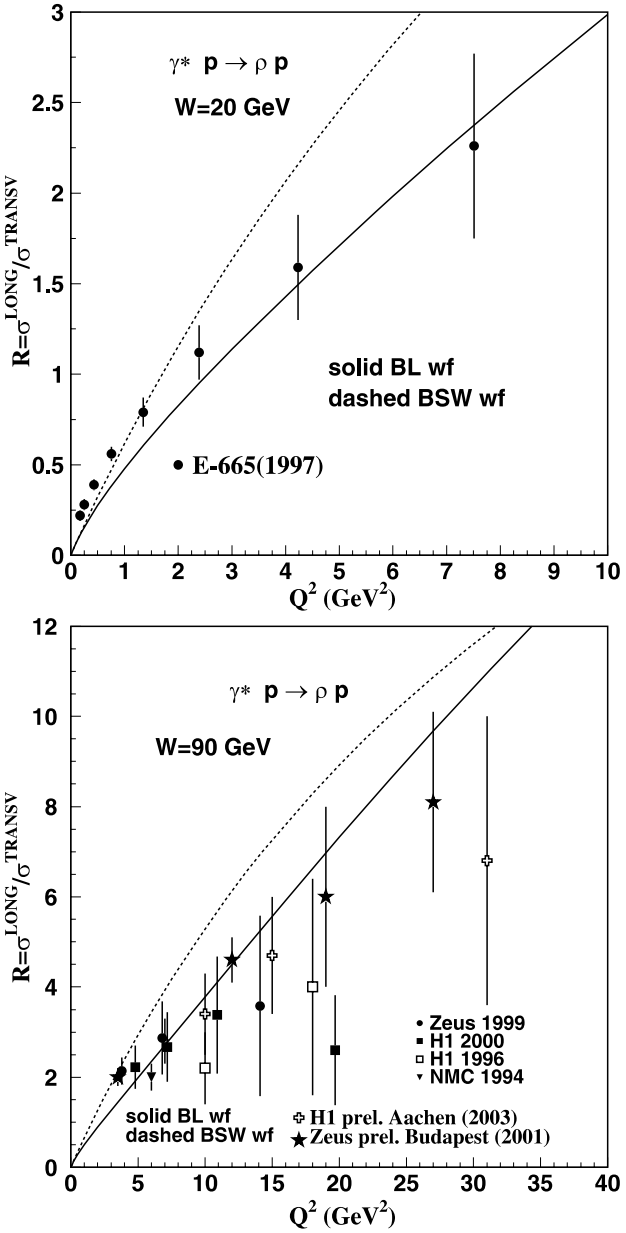

Fig. 13. The ratio R of longitudinal and transverse cross sections for ρ electroproduction as a function of Q^2 for the fixed energies of $W = 20\,\text{GeV}$, with data from E-665 [51], and $W = 90\,\text{GeV}$ with data from NMC [52, 53], Zeus [41, 54] and H1 [55–57]. The *solid* and *dashed lines* show the theoretical calculations with the BL and BSW wave functions, respectively

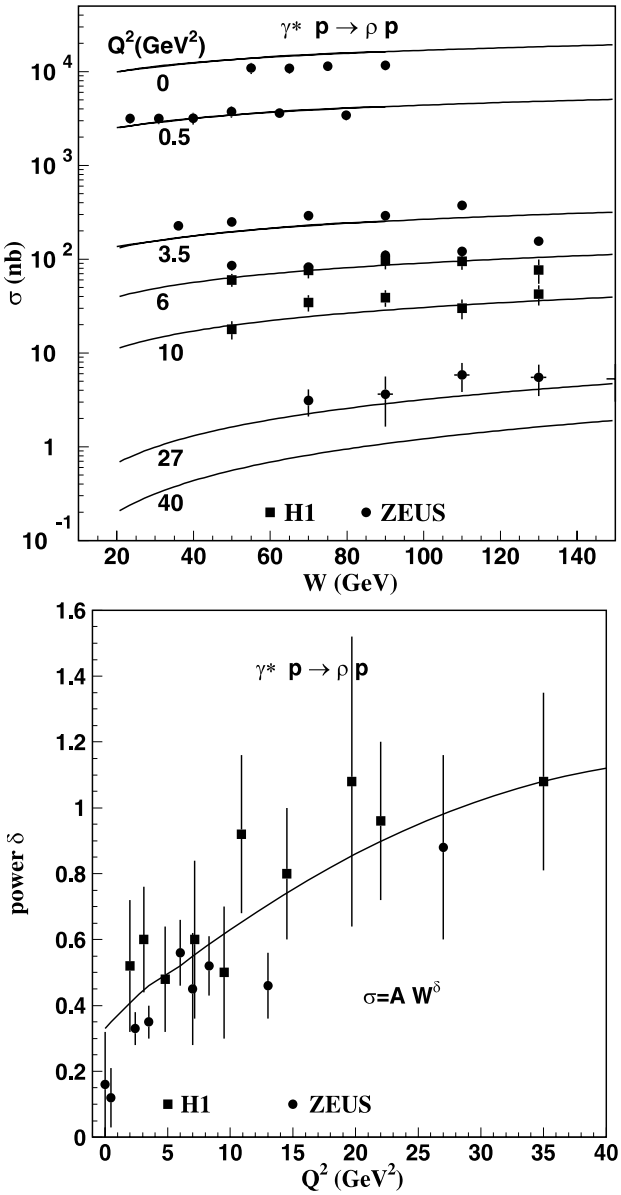

Fig. 14. The energy dependence of ρ electroproduction cross section in the region from approximately 30 to 130 GeV. The *solid lines* show our theoretical calculations for several values of Q^2, and the data are from the Zeus [41, 54, 58] and H1 [55, 56] collaborations. The plot on the *right-hand side* shows data and theoretical values for the parameter δ of the energy dependence W^δ

$Q^2 = 0.1\,\text{GeV}^2$), and the corresponding theoretical curves. The coincidence of shapes exhibits the universality of the form factors as regards the t dependence in our model. Our prediction of a curvature in the plot of $\mathrm{d}\sigma/\mathrm{d}|t|$ seems to be confirmed by the data.

3.5 Photo- and electroproduction of the ϕ meson

The ϕ meson has a strategic place between the J/ψ and the ρ meson and may help to understand the differences in behaviour of heavy and light vector mesons and also to clarify the interplay of perturbative and nonperturbative aspects of QCD.

In Fig. 18 we show the Q^2 dependence of the integrated elastic cross section in ϕ photo- and electroproduction at $W = 75\,\text{GeV}$ [65–67], together with our theoretical calculations. As in the case of ρ electroproduction, there are indications that the data cannot be well represented by a single expression of the form of (18). The data are poorer here than in the ρ case, and it is important to investigate the possibility of a transition region in an intermediate Q^2

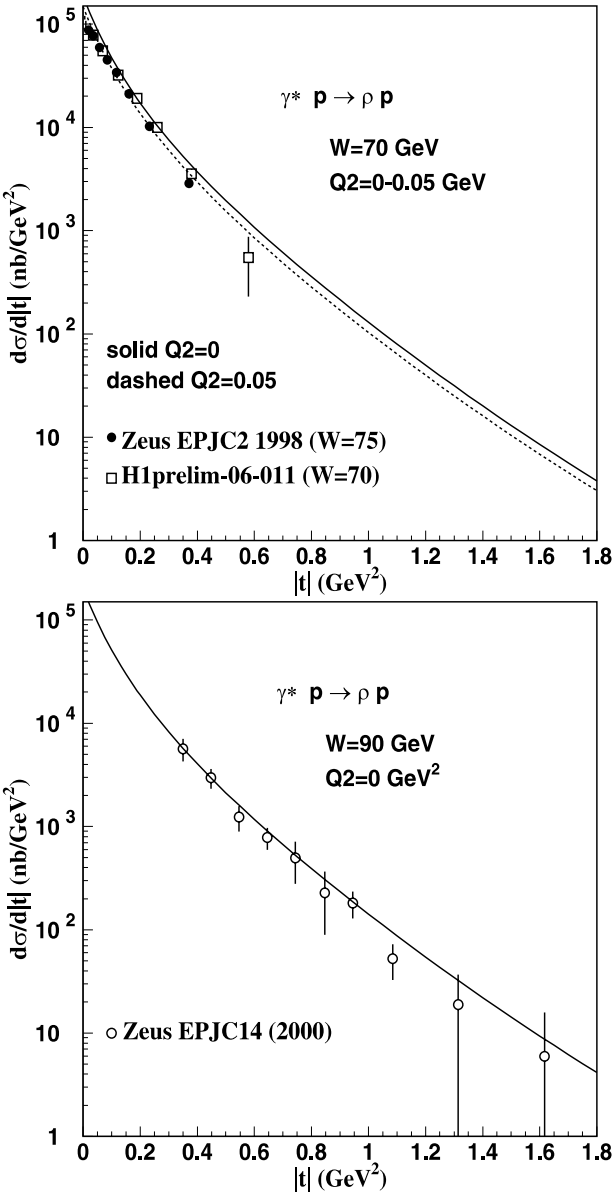

Fig. 15. Experimental data and our theoretical prediction (*solid line*) for the t dependence of the ρ photoproduction cross sections. The published data are from the Zeus collaboration, at the energies 75 GeV (low t) [58] and 94 GeV (large t) [59]. The 94 GeV data are rescaled with a factor $(90/94)^{0.16} = 0.993$ in the figure. We also include in the low-t figure preliminary information from H1 [60], extracted from their plots, for $W = 70$ GeV

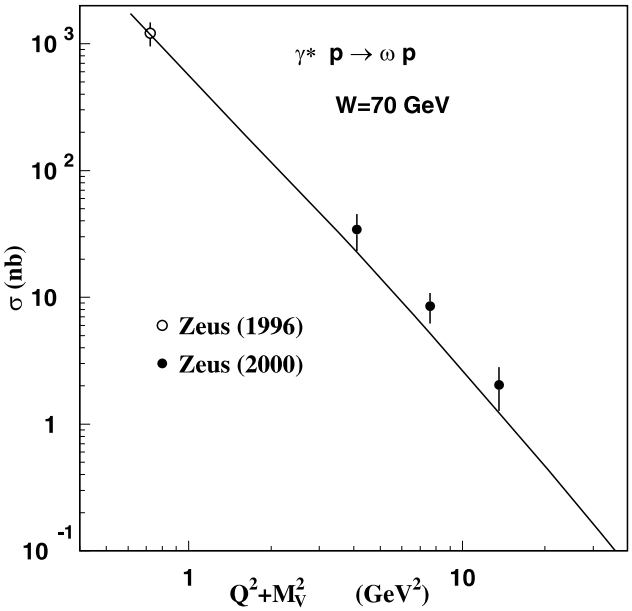

Fig. 16. Q^2 dependence of the cross section of ω elastic production [61, 62]. The *solid line* represents our calculations

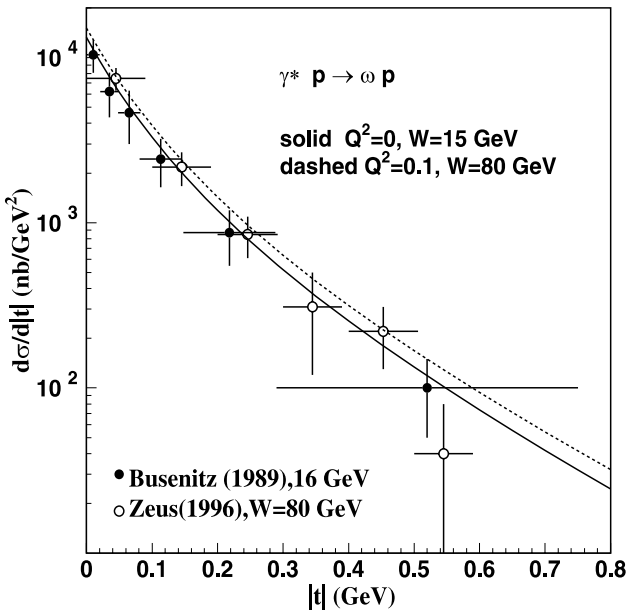

Fig. 17. t dependence of ω photoproduction cross sections [63, 64]. The plot puts together data points at the energies $W = 15$ GeV (with $Q^2 = 0$) and $W = 80$ GeV (with $Q^2 = 0.1$ GeV^2), and the corresponding theoretical curves. The curvature and the similarities of the shapes of the t distributions for two different energies and Q^2 values are characteristic features of our framework

range below 10 GeV^2 in which the normalisation and the power change values rather rapidly.

The data for the ratio $R = \sigma^{\mathrm{L}}/\sigma^{\mathrm{T}}$ for $W = 75$ GeV as a function of Q^2 [66, 67] are shown in Fig. 19, together with our results with BL and BSW wave functions. The calculations exhibit, as in the ρ meson case, the sensitivity of the ratio R to details of the wave functions. Offering a reference for the two kinds of calculation, the plot also shows (dotted line) a fit of the data, made by experimentalists.

The effective power $\delta(Q^2)$ describing the energy dependence as W^{δ} in ϕ electroproduction [67] is shown in Fig. 20, and it is compared with our results using the two-pomeron model. The theoretical Q^2 dependence is similar to that of J/ψ and ρ production, whereas the experimental points, with large errors, indicate a flatter behaviour. Obviously more data are necessary.

Our calculations give very good descriptions for the Q^2 dependence of the differential elastic cross section in the

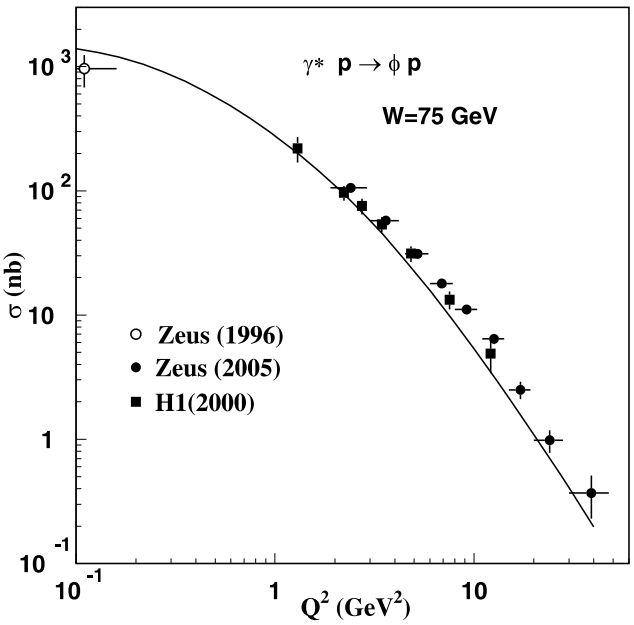

Fig. 18. Q^2 dependence of the ϕ production cross sections at $W = 75$ GeV and our theoretical description. The data are from Zeus [65, 67] and H1 [66]

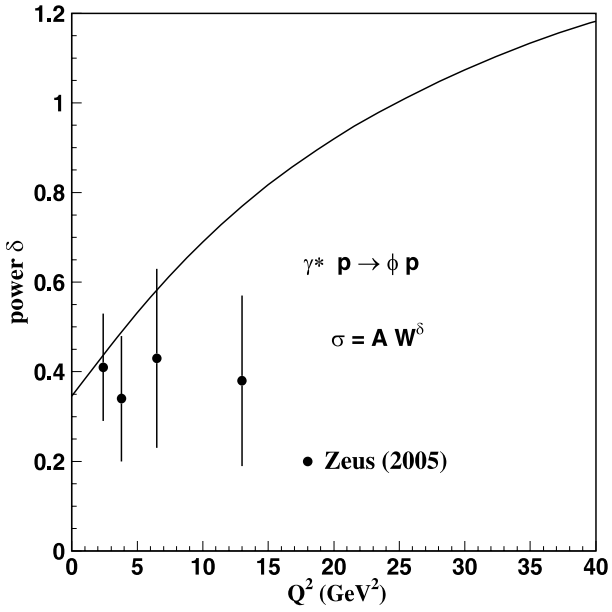

Fig. 20. The effective power δ parameter governing the energy dependence of ϕ electroproduction. The data are from Zeus [67], the *solid line* is our theoretical result

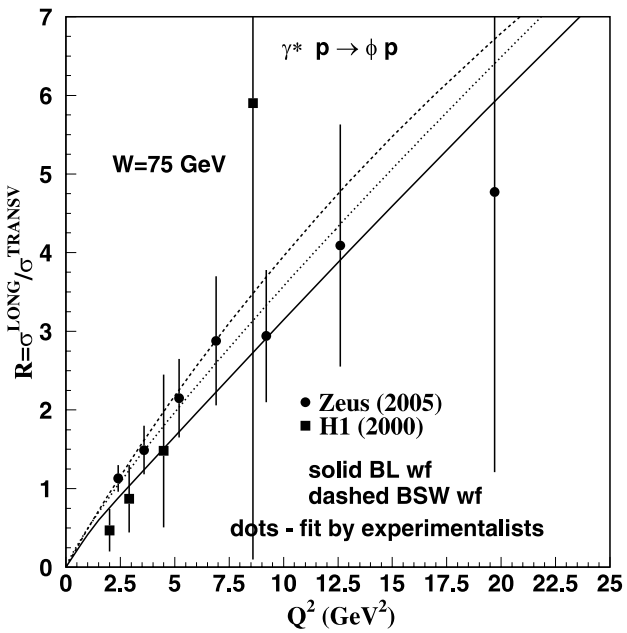

Fig. 19. Q^2 dependence of the ratio $R = \sigma^{\mathrm{L}}/\sigma^{\mathrm{T}}$ in ϕ electroproduction [66, 67] at the fixed energy of $W = 75$ GeV. The *solid* and *dashed lines* represent our calculations with BL (*solid*) and BSW (*dashed*) wave functions; the *dotted line* is a fit of the form $R = 0.51(Q^2/M^2)^{0.86}$

forward directions in ϕ electroproduction, as it does in the J/ψ case. Figure 21 shows the comparison with the experimental data [67].

There are no published measurements of $\mathrm{d}\sigma/\mathrm{d}|t|$ in ϕ production for nonzero Q^2. The Zeus photoproduction data at 94 GeV [59, 65] are shown in Fig. 22. Our theoretical calculations give a very satisfactory description.

3.6 Results concerning several vector mesons

The quantitative predictions made in a unique way for different kinds of vector mesons cover several scales of magnitudes in the cross sections. This global coverage is exhibited in Fig. 23. The same global description is given for the forward differential cross section shown in Fig. 24. In this figure the charge factors squared, $\hat{e}_V^2$, see (8), for each kind of meson are extracted, making the quantities almost universal in a $Q^2 + M_V^2$ plot. However, the universality is only approximate, and our calculation correctly predicts the observed displacements.

The data on the energy dependence of the integrated cross sections for the ρ, ϕ and ψ mesons have been presented and compared to the theoretical predictions for each case. The parameter $\delta(Q^2)$ of the suggested simple energy dependence

$$\sigma(Q^2) = \mathrm{Const.} \times W^{\delta(Q^2)}$$

has also been given in each case. This parametrisation is an approximation valid in a limited energy range, since the true energy dependence in our calculation is determined by the two-pomeron scheme, but it is considered useful in practice.

We then evaluate δ using the energy range $W =$ 20–100 GeV, for all values of Q^2. The results are put together in Fig. 25. We note that all curves start at the minimum value 4×0.08 at the same unphysical point $Q^2 + M_V^2 = 0$ and all are asymptotic to $\delta = 4 \times 0.42$ as Q^2 in-

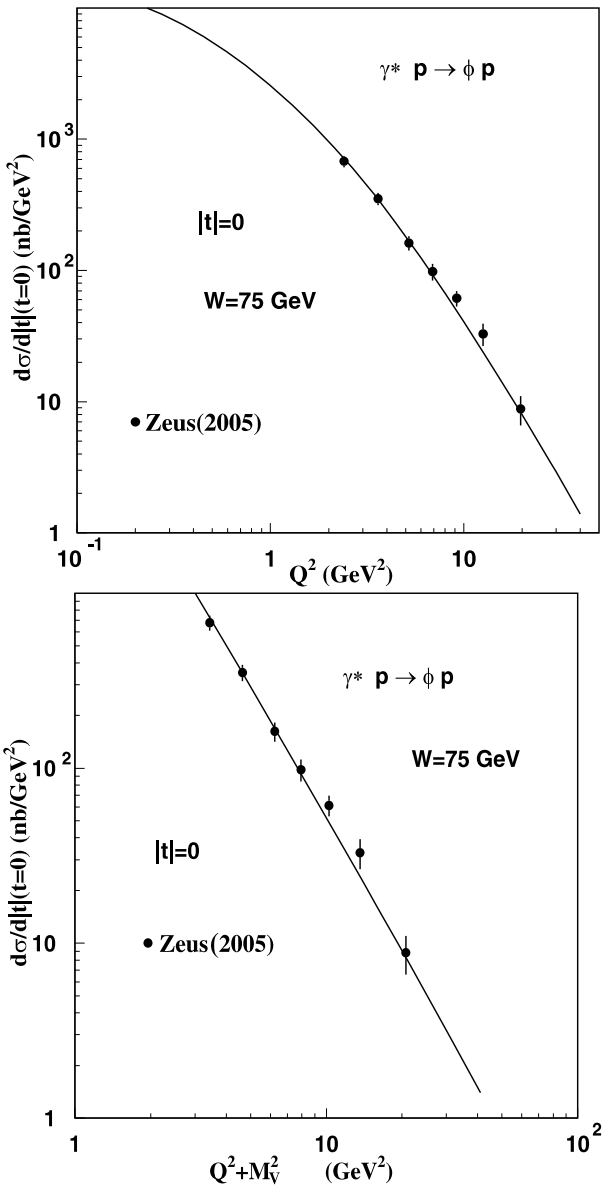

Fig. 21. Q^2 dependence of the differential cross sections of ϕ elastic in the forward direction. The *solid lines* represent our calculation. The second plot contains the same information, showing the typical behaviour of a straight line in the variable $Q^2 + M_V^2$

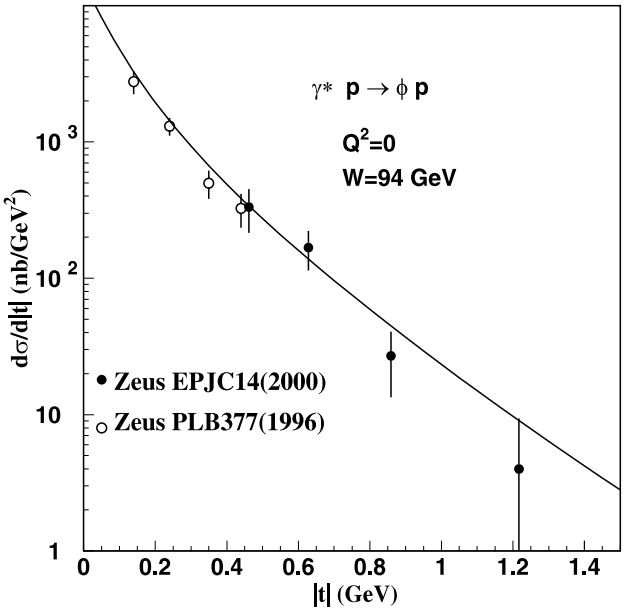

Fig. 22. t dependence of the ϕ photoproduction cross sections and its theoretical description in our nonperturbative calculation with the stochastic vacuum model. The published data are from the Zeus collaboration, at the energy 94 GeV, first at low t [65] and then at larger t [59]

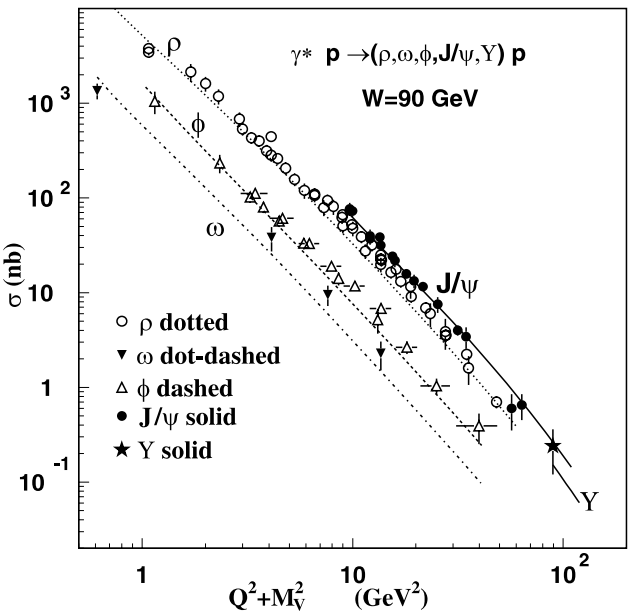

Fig. 23. Integrated elastic cross sections for all vector mesons at $W = 90$ GeV, as functions of $Q^2 + M_V^2$. The *lines* represent our theoretical calculations

creases. We then have the following form of the parametrisation:

$$\delta(Q^2) = 0.32 + 1.36 \frac{(1+Q^2/M_V^2)^n}{A + (1+Q^2/M_V^2)^n}\,, \qquad (22)$$

and the values for A and n are given in Table 1.

Our model gives definite predictions for the t dependence in the differential cross sections. The shape can be conveniently represented by the form given in (21). Figure 26 shows the form factor $F(|t|)$ for all vector mesons at the fixed energy $W = 90$ GeV.

The curvature in the log graph is a prediction of our framework. The values of the parameters as functions of Q^2 are shown in one of the plots. In Table 2 some numerical values of a, b are given.

As the virtuality Q^2 grows, the ranges of the overlap functions decrease, and the electroproduction cross sections of all mesons become flatter, all tending together to the shape characteristic of the Υ meson, with the same limiting values, $a = 4.02\,\mathrm{GeV}^2$ and $b = 1.60\,\mathrm{GeV}^2$, for the

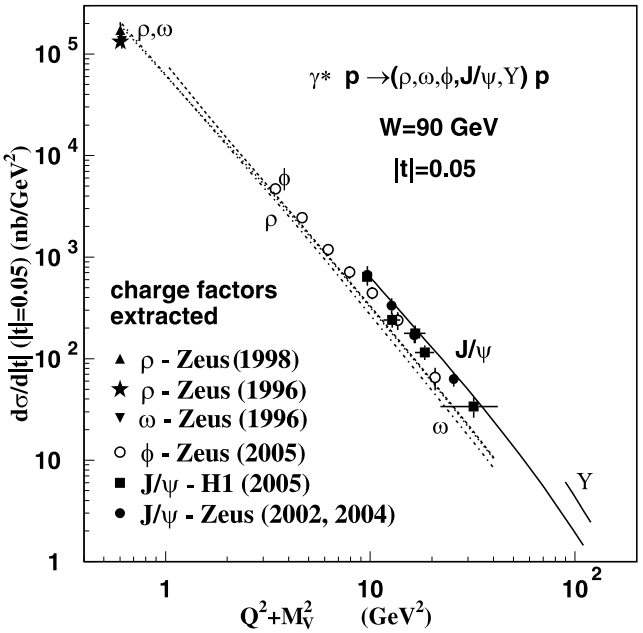

Fig. 24. Differential cross sections in a forward direction for all vector mesons at $W = 90$ GeV, as functions of $Q^2 + M_V^2$, with extraction of charge factors . The *lines* represent the theoretical calculations with the stochastic vacuum model as in Fig. 23

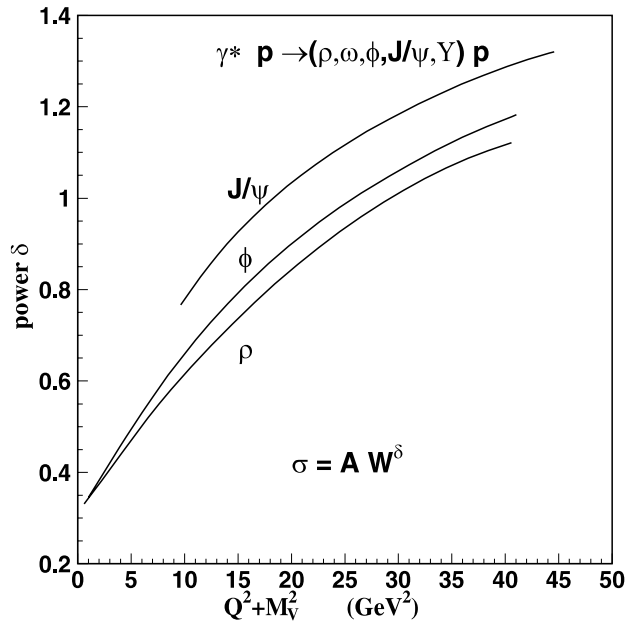

Fig. 25. The parameter $\delta(Q^2)$ of the energy dependence of the cross sections

Table 1. Values of A and n in the exponent $\delta(Q^2)$ from (22)

Meson	ρ	ϕ	J/ψ	Υ
A	124.926	51.9183	2.0624	0.9307
n	1.239	1.239	1.12	0.22

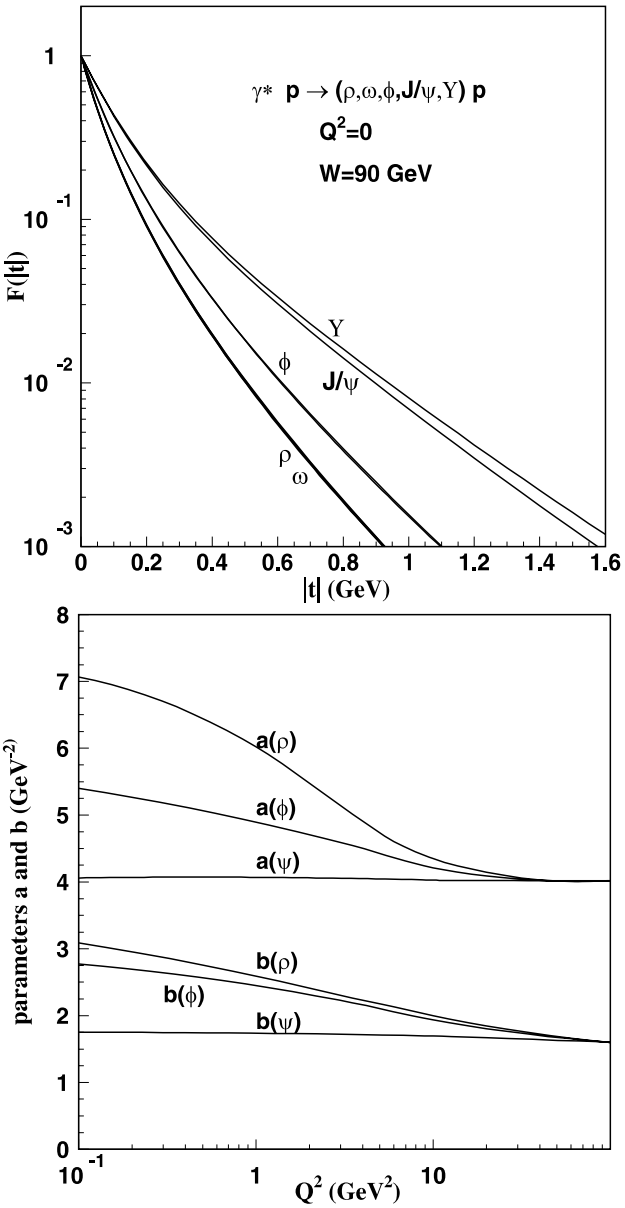

Fig. 26. Form factor $F(|t|)$ of the $|t|$ distribution in the elastic differential cross sections for photoproduction of vector mesons, with the characteristic curvatures in the log plot predicted in our calculations. The curves follow the shapes given by (21), with $a(Q^2)$ and $b(Q^2)$ represented in the second figure. Specific numerical values of the parameters for $Q^2 = 0,\ 10$ and 20 GeV^2 are given in Table 2. The values in the limit of very large Q^2 are $a = 4.02$ GeV^{-2} and $b = 1.60$ GeV^{-2}

parameters. The limiting shape of the distribution for very large Q^2 is illustrated in Fig. 27, where we see all vector mesons superposed. In the figure we draw the piece of straight line representing the slope considered as the average for the interval from $|t| = 0$ to $|t| = 0.2$ GeV^2. As indicated inside the plots, the calculations of the form factors presented in the figures are made for $W = 90$ GeV. In the second plot presented in Fig. 27 we show the (absence of the) dependence of the form factor on the energy W. Thus we predict that there is no shrinking of the forward peak in

Table 2. Some values (in GeV^{-2}) of the parameters a and b of $\frac{\mathrm{d}\sigma}{\mathrm{d}|t|} = \left[\frac{\mathrm{d}\sigma}{\mathrm{d}|t|}\right]_{t=0} \times \frac{\mathrm{e}^{-b|t|}}{(1+a|t|)^2}$ in (21). The full Q^2 dependence is shown in Fig. 26

	$Q^2=0$		$Q^2=10\,\mathrm{GeV}^2$		$Q^2=20\,\mathrm{GeV}^2$	
Meson	a	b	a	b	a	b
$\rho(770)$	7.06	3.09	4.349	1.996	4.145	1.846
$\omega(782)$	7.20	3.08	4.323	1.990	4.141	1.835
$\phi(1020)$	5.40	2.77	4.211	1.934	4.091	1.807
$J/\psi(1S)$	4.06	1.75	4.026	1.696	4.022	1.670
$\Upsilon(1S)$	4.03	1.61	4.027	1.606	4.025	1.604

$\mathrm{d}\sigma/\mathrm{d}|t|$ as the energy increases. The experimental data are not yet sufficient to test all these predictions.

4 Relation with other approaches

Our work runs parallel to other developments, of mainly nonperturbative nature, based on colour dipole dynamics. These treatments, which started with studies of the $\gamma^* p$ total cross section [68] and soon were extended to diffractive deep inelastic scattering [69], are based on the assumption that the photon fluctuates into a $q\bar{q}$ pair, which then scatters with the proton, according to a properly built dipole cross section σ_{dipole}. The $q\bar{q}$ dipole then recombines to form again a photon, or eventually a vector meson, in the final state. Photons, either real or virtual, enter in a well defined way through their QED wave functions, and the dipole cross section is built with the necessary ingredients to describe the observed phenomenology and, as much as possible, to follow QCD prescriptions. The proton structure is introduced to give an impact parameter dependence that allows for the description of the t dependence in a predictable way.

Concerns with the observed saturation effects in the Q^2 and x dependences led to an ansatz for σ_{dipole} of the form

$$\sigma_{\mathrm{dipole}}(x,r) = \sigma_0\big(1-\exp\left(-r^2 Q_{\mathrm{s}}^2(x)/4\right)\big)\,, \qquad (23)$$

where σ_0 is a constant and $Q_{\mathrm{s}}(x)$ denotes the x dependent saturation scale. For processes governed by quarks of mass m_f, the Bjorken scale x is taken as

$$x_{m_f} = \frac{Q^2}{Q^2+W^2}\left(1+\frac{4m_f^2}{Q^2}\right)\,. \qquad (24)$$

This kind of dipole cross section worked well for what it was aimed for: giving a description of the HERA data on inclusive (related to F_2) and diffractive $\gamma^* p$ processes. In an effort to improve the model including scaling violations and QCD evolution, Bartels, Golec-Biernat and Kowalski [70] replaced the saturation scale Q_{s}^2 by a gluon density obeying the equation of DGLAP evolution. The interplay between saturation and evolution improved the fits of the F_2 data, especially for large Q^2.

Another improvement of the original saturation model came with the color glass condensate model [71], dealing with the question of the low-x behaviour near the saturation region through BFKL dynamics. These calculations were successful as an extension of the model, although they did not include charm contributions.

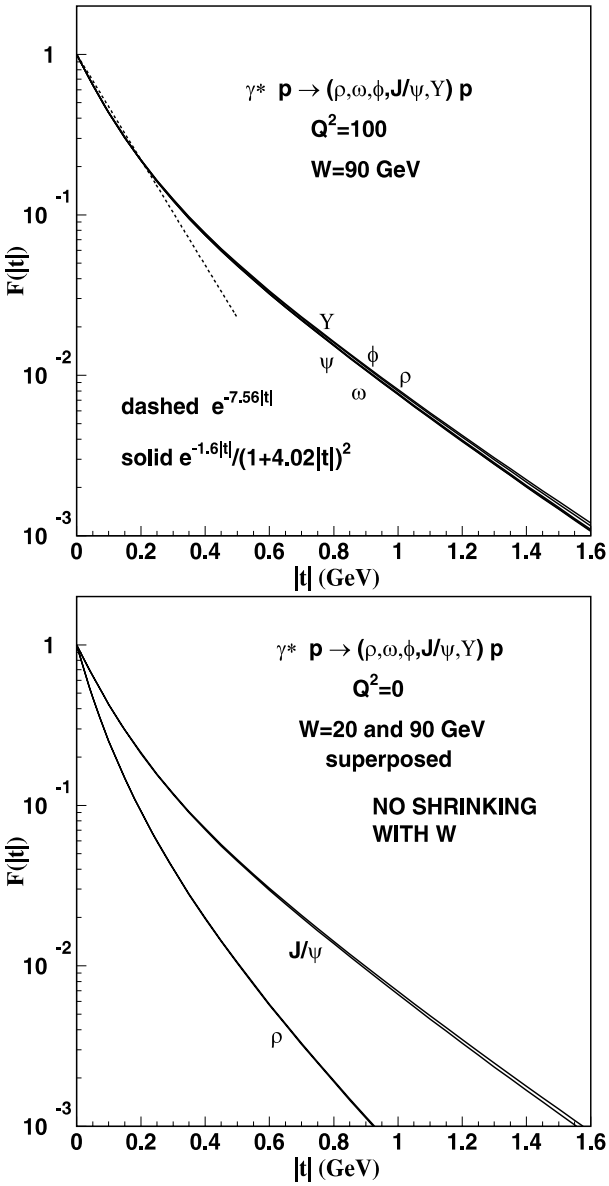

Fig. 27. The plot on the *left-hand side* shows the shape of the $|t|$ distribution in the differential cross section for electroproduction common to all vector mesons for very large Q^2. The *straight line* passes through the points $|t|$ equal to zero and $0.2\,\mathrm{GeV}^2$, indicating the average slope that would be measured in this limit. The plot on the *right-hand side* shows that $F(|t|)$ does not depend significantly on the energy, and thus measurement of slopes at fixed Q^2 would give a constant value for each vector meson

An important line of development of the phenomenological color dipole models came with the introduction of effects of the proton shape, with an explicit impact parameter dependence in the dipole scattering, by Kowalski and Teaney [72], and consequently with the possibility of the treatment of the t distributions.

This work was extended by Kowalski, Motyka and Watt to the description of photo- and electroproduction of vector mesons [73], going beyond F_2 and DVCS. These authors use the same kind of dipole cross section as KT , based on Glauber–Mueller:

$$\frac{\mathrm{d}\sigma_{\mathrm{dipole}}}{\mathrm{d}^2\mathbf{b}} = 2\left[1-\exp\left(-\frac{\pi^2}{2N_c}r^2\alpha_{\mathrm{s}}(\mu^2)xg(x,\mu^2)T(b)\right)\right]. \tag{25}$$

The scale μ^2 is related to the dipole size, and the gluon density is evolved from μ_0^2 to μ^2 using LO DGLAP evolution without quarks. Application of this model requires a number of ingredients and parameters, as the form of the gluon density at μ_0, the effective x for heavy quarks, the proton shape $T(b)$, and the b dependence in the form of σ_{dipole}. The paper mentioned describes part of the recent HERA data on photo- and electroproduction of vector mesons that we discuss in the present paper, with an interesting similarity of results.

A fundamental and original approach for the implementation of the dipole treatment of vector meson production, which provides the framework for the present work, was developed by the Heidelberg group [21, 25, 26]. This approach calculates the basic loop–loop interaction using the stochastic vacuum model [13, 14, 20], which is a genuine nonperturbative treatment that allows for connections with other branches of nonperturbative QCD, especially with the fundamental and striking feature of confinement. The method is based on functional methods [11] and has been used recently for investigations on the foundations and limitations of the dipole model [12, 74, 75].

The same approach using the loop–loop amplitude and the stochastic vacuum model was used consistently by Donnachie and Dosch for calculations of DVCS [35] and structure functions [36] .

The treatment of photoproduction of all vector mesons through a dipole pomeron model respecting the unitarity bounds by Martynov, Predazzi and Prokudin [76] nicely described the W and t dependences in elastic photoproduction processes and was soon extended to electroproduction [77].

A separation of hard (small) and soft (large) dipole interactions, testing several prescriptions for the dipole cross section and several forms of wave function, was used by Forshaw, Sandapen and Shaw [78, 79] to describe the energy and Q^2 dependences of the total $\gamma^* p$ cross section, diffractive electroproduction, DVCS and exclusive J/ψ electroproduction. The separation of dipoles in two classes is similar to the two-pomeron model adopted in the present work.

As a whole, these nonperturbative models for γ^* induced processes, all based on the dipole picture, are phenomenologically satisfactory. This is not surprising, since it has already been shown [18] that many features of these processes, particularly the Q^2 dependence, are reproduced by the overlap of the light cone wave functions of photons and mesons folded with the basic r^2 behaviour of the dipole cross sections.

Unfortunately, the presently available data are not sufficient to discriminate details of the different approaches, particularly in the incorporation of the energy dependence.

5 Summary and discussion

We have shown the predictions for elastic electroproduction processes using two basic ingredients:

1) the overlaps of photon and meson wave functions, written as packets of quark–antiquark dipoles, with protons described also as packets of dipoles (in a convenient diquark model for the nucleon),
2) the interaction of two dipoles described in terms of geometric variables in an impact parameter representation of the amplitudes based on nonperturbative properties of the QCD gluon field.

These quantities put together and integrated over the distribution of dipoles in the initial and final states lead to a correct description of the data concerning all vector mesons.

In all cases the variations with energy are very well described by the Regge picture, with soft and hard pomerons coupled to large and small dipoles, respectively. We recall that in approaches mainly based on perturbation theory the energy (or x) dependence is introduced through the gluon distribution in the proton.

Each of the different mesons enter in the calculation characterised only by the masses and charges of its quark contents, and with their normalised wave function individualised only by the corresponding electromagnetic decay rate (related to the value of the wave function at the origin).

The specific nonperturbative input is the stochastic vacuum model, which has been successfully applied in many fields, from hadron spectroscopy to high energy scattering. The basic interaction of two dipoles depends only on universal features of the QCD field, which are the numerical values of the gluon condensate and of the correlation length of the finite range correlations. These two quantities have been determined by lattice investigations and tested independently in several instances of phenomenological use of the dipole–dipole interaction.

As has already been pointed out [18], the main features of the Q^2 dependence of electroproduction of vector mesons are contained in the overlap integral. For values of Q^2 attainable at present, this overlap integral is determined by perturbative QCD, through the photon wave function, and by nonperturbative QCD, through the meson wave function. The production of transversely polarised mesons is determined by the meson wave function even for very high values of Q^2. The importance of nonperturbative effects in vector meson production has also been stressed in [37], where the perturbative two-gluon exchange has been supplemented by an exchange of nonperturbative gluons. In our approach, which incorporates both perturbative and nonperturbative effects, we are able to give a fair overall description of all observables of vector meson production: the energy dependence, the Q^2 dependence, the ratio of longitudinal to transverse mesons and the angular distribution.

In this paper our calculations are compared to the large amount of HERA data for the $\rho, \omega, \phi, J/\psi$ and Υ mesons.

Acknowledgements. Both authors wish to thank DAAD (Germany), CNPq (Brazil) and FAPERJ (Brazil) for support of the scientific collaboration program between Heidelberg and Rio de Janeiro groups working on hadronic physics. One of the authors (EF) is grateful to CNPq (Brazil) for research fellowship and grant.

Appendix : QCD and wave function parameters

Here we recall some expressions and the numerical values of quantities used in the nonperturbative contributions, which have been unchanged for many applications.

The loop–loop scattering amplitude $S(b, W, z_1, \mathbf{R}_1, z_2 = 1/2, \mathbf{R}_2)$, determining the essential quantity $J(\mathbf{q}, W, z_1, \mathbf{R}_1)$ in (2), can be calculated using the stochastic vacuum model. The essential input parameters of this model are the correlation length a of the gauge invariant two-gluon correlator and the gluon condensate $\langle g_s^2 FF\rangle$. These quantities have been determined in lattice calculations [33]. The numerical values used in this and previous papers are

$$a = 0.346\,\mathrm{fm}\,, \quad \langle g_s^2 FF\rangle a^4 = 23.5\,. \tag{A.1}$$

The constant $\kappa = 0.74$ appearing in the correlation functions preserves its value determined by lattice calculations.

The energy dependence is based on a two-pomeron model; small dipoles with size $R < R_\mathrm{c}$ couple to the hard pomeron with an intercept $\alpha_{P\,h}(0) = 1.42$, whereas large dipoles with $R > R_\mathrm{c}$ couple to the soft pomeron with an intercept $\alpha_{P\,s}(0) = 1.08$. The transition radius R_c has been determined from the x dependence of the proton structure function: $R_\mathrm{c} = 0.22\,\mathrm{fm}$.

For the proton wave function occurring in (2) we use a diquark–quark Gaussian wave function with the transverse radius $R_P = 0.75\,\mathrm{fm}$.

The light quark masses which can simulate confinement effects in the otherwise perturbative photon wave function [25] are

$$m_u = m_d = 0.2\,\mathrm{GeV}\,, \quad m_s = 0.3\,\mathrm{GeV}\,. \tag{A.2}$$

For the heavy quarks we take the renormalised masses in the $\overline{MS}$ scheme

$$m_c = 1.25\,\mathrm{GeV}\,, \quad m_b = 4.2\,\mathrm{GeV}\,. \tag{A.3}$$

The full form of photon and vector meson wave functions used in our work, including the helicity dependences, have been presented before [16, 18], with two forms for the vector mesons: the Bauer–Stech–Wirbel (BSW) [27, 28], and the Brodsky and Lepage (BL) [29, 30] wave functions, where the separate r, z dependences are respectively

$$\phi_\mathrm{BSW}(z,r) = \frac{N}{\sqrt{4\pi}}\sqrt{z\bar z}\exp\left[-\frac{M_V^2(z-\frac12)^2}{2\omega^2}\right] \times \exp\left[-\frac{\omega^2 r^2}{2}\right]\,, \tag{A.4}$$

(here M_V represents the vector meson mass) and

$$\phi_\mathrm{BL}(z,r) = \frac{N}{\sqrt{4\pi}}\exp\left[-\frac{m_f^2(z-\frac12)^2}{2z\bar z\omega^2}\right]\exp\left[-2z\bar z\omega^2 r^2\right]\,, \tag{A.5}$$

with m_f representing the quark mass.

The parameters N (normalisation) and ω (which fixes the extension) are determined using the electromagnetic decay rates of the vector mesons. Their values are collected [18] in Table 3.

After summation over the helicity indices, the overlaps of the photon and vector meson wave functions

$$\rho_{\gamma^* V,\lambda}(Q^2; z_1, \mathbf{R}_1) = \psi_{V\lambda}(z_1, \mathbf{R}_1)^* \psi_{\gamma^*\lambda}(Q^2; z_1, \mathbf{R}_1) \tag{A.6}$$

that appear in (1) are given by

$$\begin{aligned}&\rho_{\gamma^* V,\pm1;\mathrm{BSW}}(Q^2; z, r)\\ &= \hat{\mathrm{e}}_V \frac{\sqrt{6\alpha}}{2\pi}\left(\epsilon_f\omega^2 r\left[z^2+\bar z^2\right]K_1(\epsilon_f r) + m_f^2 K_0(\epsilon_f r)\right)\\ &\quad\times\phi_\mathrm{BSW}(z,r)\end{aligned} \tag{A.7}$$

and

$$\begin{aligned}&\rho_{\gamma^* V,\pm1;\mathrm{BL}}(Q^2; z, r)\\ &= \hat{\mathrm{e}}_V \frac{\sqrt{6\alpha}}{2\pi}\left(4\epsilon_f\omega^2 r z\bar z\left[z^2+\bar z^2\right]K_1(\epsilon_f r) + m_f^2 K_0(\epsilon_f r)\right)\\ &\quad\times\phi_\mathrm{BL}(z,r)\,,\end{aligned} \tag{A.8}$$

for the transverse case, and the BSW and BL wave functions, respectively. For the longitudinal case we can write

Table 3. Parameters of the vector meson wave functions

		BSW				BL			
		transverse		longitudinal		transverse		longitudinal	
Meson	f_V (GeV)	ω (GeV)	N	ω (GeV)	N	ω (GeV)	N	ω (GeV)	N
$\rho(770)$	0.15346	0.2159	5.2082	0.3318	4.4794	0.2778	2.0766	0.3434	1.8399
$\omega(782)$	0.04588	0.2084	5.1770	0.3033	4.5451	0.2618	2.0469	0.3088	1.8605
$\phi(1020)$	0.07592	0.2568	4.6315	0.3549	4.6153	0.3113	1.9189	0.3642	1.9201
$J/\psi(1S)$	0.26714	0.5770	3.1574	0.6759	5.1395	0.6299	1.4599	0.6980	2.3002
$\Upsilon(1S)$	0.23607	1.2850	2.4821	1.3582	5.9416	1.3250	1.1781	1.3742	2.7779

jointly

$$\rho_{\gamma^* V,0;X}(Q^2;z,r) = -16\hat{e}_V \frac{\sqrt{3\alpha}}{2\pi}\omega z^2\bar{z}^2 Q K_0(\epsilon_f r)\phi_X(z,r)\,, \tag{A.9}$$

with X standing for BSW or BL. The effective quark charges $\hat{e}_V$ are $1/\sqrt{2}$ for ρ, $1/3\sqrt{2}$ for ω, $-1/3$ for ϕ and Υ and $2/3$ for ψ. The quantity

$$\epsilon_f = \sqrt{z(1-z)Q^2 + m_f^2} \tag{A.10}$$

and the modified Bessel functions are introduced by the photon wave functions.

References

1. A. Donnachie, P. Landshoff, Phys. Lett. B **311**, 403 (1987)
2. M.G. Ryskin, Z. Phys. C **57**, 89 (1993)
3. S.J. Brodsky, L. Frankfurt, J.F. Gunion, A.H. Mueller, M. Strikman, Phys. Rev. D **50**, 3134 (1994)
4. M.G. Ryskin, R.G. Roberts, A.D. Martin, E.M. Levin, Z. Phys. C **76**, 231 (1997)
5. E. Gotsman, E. Ferreira, E. Levin, U. Maor, E. Naftali, Phys. Lett. B **503**, 277 (2001)
6. E. Gotsman, E. Levin, U. Maor, E. Naftali, Phys. Lett. B **532**, 37 (2002)
7. L. Frankfurt, W. Koepf, M. Strikman, Phys. Rev. D **54**, 3194 (1996)
8. L. Frankfurt, W. Koepf, M. Strikman, Phys. Rev. D **57**, 512 (1998)
9. A.D. Martin, M.G. Ryskin, T. Teubner, Phys. Rev. D **62**, 014022 (2000)
10. E. Gotsman, E. Levin, M. Lublinsky, U. Maor, E. Naftali, Acta Phys. Pol. B **34**, 3255 (2003)
11. O. Nachtmann, Ann. Phys. **209**, 436 (1991)
12. C. Ewerz, O. Nachtmann, hep-ph/0404254 and hep-ph/0511051
13. H.G. Dosch, Phys. Lett. B **190**, 177 (1987)
14. H.G. Dosch, Y.A. Simonov, Phys. Lett. B **205**, 339 (1988)
15. A. Donnachie, P.V. Landshoff, Phys. Lett. B **437**, 408 (1998)
16. H.G. Dosch, E. Ferreira, Eur. Phys. J. C **29**, 45 (2003)
17. H.G. Dosch, E. Ferreira, Phys. Lett. B **576**, 83 (2003)
18. E. Ferreira, V.L. Baltar, Nucl. Phys. A **748**, 608 (2005) [arXiv:hep-ph/0409021]
19. H.G. Dosch, A. Kramer , Phys. Lett. B **252**, 669 (1990)
20. H.G. Dosch, E. Ferreira, A. Kramer, Phys. Rev. D **50**, 1992 (1994) [arXiv:hep-ph/9405237]
21. H.G. Dosch, T. Gousset, G. Kulzinger, H.J. Pirner, Phys. Rev. D **55**, 2602 (1997)
22. B.Z. Kopeliovich, J. Nemchik, N.N. Nikolaev, B.G. Zakharov, Phys. Lett. B **324**, 469 (1994)
23. B.Z. Kopeliovich, Phys. Lett. B **309**, 179 (1993)
24. B. Blaettel, G. Baym, L.L. Frankfurt, M. Strikman, Phys. Rev. Lett. **70**, 896 (1993)
25. H.G. Dosch, T. Gousset, H.J. Pirner, Phys. Rev. D **57**, 1666 (1998)
26. G. Kulzinger, H.G. Dosch, H.J. Pirner, Eur. Phys. J. C **7**, 73 (1999)
27. M. Bauer, B. Stech, M. Wirbel, Z. Phys. C **34**, 103 (1987)
28. M. Bauer, Z. Phys. C **29**, 637 (1985)
29. G.P. Lepage, S.J. Brodsky, Phys. Rev. D **22**, 2157 (1980)
30. S.J. Brodsky, H.C. Pauli, S.S. Pinsky, Phys. Rep. **301**, 299 (1998)
31. G. Dosch, S. Donnachie, P. Landshoff, O. Nachtmann, Pomeron Physics and QCD (Cambridge University Press, Cambridge, England, 2002)
32. A. Di Giacomo, H.G. Dosch, V.I. Shevchenko, Y.A. Simonov, Phys. Rep. **372**, 319 (2002)
33. M. D'Elia, A. Di Giacomo, E. Meggiolaro, Nucl. Phys. Proc. Suppl. **73**, 515 (1999)
34. A. Donnachie, H.G. Dosch, M. Rueter, Eur. Phys. J. C **13**, 141 (2000)
35. A. Donnachie, H.G. Dosch, Phys. Lett. B **502**, 74 (2001) [arXiv:hep-ph/0010227]
36. A. Donnachie, H.G. Dosch, Phys. Rev. D **65**, 014019 (2002) [arXiv:hep-ph/0106169]
37. A. Donnachie, J. Gravelis, G. Shaw, Phys. Rev. D **63**, 114013 (2001)
38. ZEUS Collaboration, S. Chekanov et al., Eur. Phys. J. C **24**, 345 (2002)
39. ZEUS Collaboration, S. Chekanov et al., Nucl. Phys. B **695**, 3 (2004)
40. H1 Collaboration, A. Aktas et al., Eur. Phys. J. C **46**, 585 (2006)
41. ZEUS Collaboration, J. Breitweg et al., Eur. Phys. J. C **6**, 603 (1999)
42. H1 Collaboration, C. Adloff et al., Eur. Phys. J. C **10**, 373 (1999)
43. E-401 Collaboration, M. Binkley et al., Phys. Rev. Lett. **49**, 73 (1982)
44. E-516 Collaboration, B.H. Denby et al., Phys. Rev. Lett. **52**, 795 (1984)
45. Zeus Collaboration, J. Breitweg et al., Phys. Lett. B **437**, 432 (1998)
46. H1 Collaboration, C. Adloff et al., Phys. Lett. B **483**, 23 (2000)
47. R.M. Egloff et al., Phys. Rev. Lett. **43**, 657 (1979)
48. Chio Collaboration, W.D. Shambroom et al., Phys. Rev. D **26**, 1 (1982)
49. EMC Collaboration, J.J. Aubert et al., Phys. Lett. B **161**, 203 (1985)
50. J. Ashman et al., Z. Phys. C **39**, 169 (1988)
51. E-665 experiment, M.R. Adams et al., Z. Phys. C **74**, 237 (1997)
52. NMC Collaboration, M. Arneodo et al., Nucl. Phys. B **429**, 503 (1994)
53. P. Amaudruz et al., Z. Phys. C **54**, 239 (1992)
54. ZEUS Collaboration, Preliminary, Budapest Conference 2001
55. H1 Collaboration, C. Adloff et al., Eur. Phys. J. C **13**, 371 (2000)
56. H1 Collaboration, Preliminary, Aachen Conference 2003
57. H1 Collaboration, S. Aid et al., Nucl. Phys. B **468**, 3 (1996)
58. Zeus Collaboration, J. Breitweg et al., Eur. Phys. J. C **2**, 247 (1998)
59. Zeus Collaboration, J. Breitweg et al., Eur. Phys. J. C **14**, 213 (2000)
60. H1prelim-06-011, presented in DIS-2006, Tsukuba, Japan, April 2006
61. Zeus Collaboration, M. Derrick et al., Z. Phys. C **73**, 73 (1996)

62. Zeus Collaboration, J. Breitweg et al., Phys. Lett. B **487**, 273 (2000)
63. FNAL-401, J. Busenitz et al., Phys. Rev. D **40**, 1 (1989)
64. ZEUS Collaboration, M. Derrick et al., Z. Phys. C **73**, 73 (1996)
65. Zeus Collaboration, M. Derrick et al., Phys. Lett. B **377**, 259 (1996)
66. H1 Collaboration, C. Adloff et al., Phys. Lett. B **483**, 360 (2000)
67. ZEUS Collaboration, S. Chekanov et al., Nucl. Phys. B **718**, 3 (2005)
68. K. Golec-Biernat, M. Wusthoff, Phys. Rev. D **60**, 11 402 (1999) [arXiv:hep-ph/9903358]
69. K. Golec-Biernat, M. Wusthoff, Phys. Rev. D **59**, 01 401 (1999) [arXiv:hep-ph/9807513]
70. J. Bartels, K. Golec-Biernat, H. Kowalski, Phys. Rev. D **66**, 01 400 (2002) [arXiv:hep-ph/0203258]
71. E. Iancu, K. Itakura, S. Munier, Phys. Lett. B **590**, 19 (2004) [arXiv:hep-ph/0310338]
72. H. Kowalski, D. Teaney, Phys. Rev. D **68**, 11 400 (2003) [arXiv:hep-ph/0304189]
73. H. Kowalski, L. Motyka, G. Watt, Phys. Rev. D **74**, 07 401 (2006) [arXiv:hep-ph/0606272]
74. C. Ewerz, O. Nachtmann, arXiv:hep-ph/0604087
75. C. Ewerz, O. Nachtmann, arXiv:hep-ph/0611076
76. E. Martynov, E. Predazzi, A. Prokudin, Phys. Rev. D **67**, 07 402 (2003) [arXiv:hep-ph/0207272]
77. R. Fiore, L.L. Jenkovszky, F. Paccanoni, A. Prokudin, Phys. Rev. D **68**, 01 400 (2003) [arXiv:hep-ph/0302195]
78. J.R. Forshaw, R. Sandapen, G. Shaw, Phys. Rev. D **69**, 09 401 (2004) [arXiv:hep-ph/0312172]
79. J.R. Forshaw, R. Sandapen, G. Shaw, JHEP **0611**, 02 (2006) [arXiv:hep-ph/0608161]